Investigation of $\Lambda_b \to \Lambda_c \ell^- \bar{\nu}_\ell$ decays in the perturbative QCD approach

Ying Li,[1,*] Jie Chen,[1] Ya-Xin Wang,[2] and Zhi-Tian Zou[1,†]
[1]Department of Physics, Yantai University, Yantai 264005, China
[2]Institute of Particle Physics and Key Laboratory of Quark and Lepton Physics (MOE), Central China Normal University, Wuhan, Hubei 430079, China

(Received 16 September 2025; accepted 2 January 2026; published 20 January 2026)

We investigate the semileptonic decays $\Lambda_b \to \Lambda_c \ell^- \bar{\nu}_\ell$ (with $\ell = e, \mu, \tau$) within the framework of perturbative QCD. The six independent $\Lambda_b \to \Lambda_c$ transition form factors are first calculated in the low-q^2 region using the k_T factorization approach. These are then extrapolated to the full physical q^2 range via the model-independent z expansion, incorporating recent lattice QCD results at high q^2. Based on the obtained form factors, we compute the branching fractions of $\Lambda_b \to \Lambda_c \ell^- \bar{\nu}_\ell$ decays. Our prediction for the lepton flavor universality ratio, $\mathcal{R}_{\Lambda_c} = 0.29^{+0.12}_{-0.11}$, is slightly larger than the latest experimental measurement. In addition, we analyze several angular observables, including forward-backward asymmetries, lepton-side convexity parameters, and polarization asymmetries. These results offer valuable theoretical input for current and future experimental investigations of semileptonic heavy-to-heavy baryon transitions.

DOI: 10.1103/8ztx-56ys

I. INTRODUCTION

Semileptonic decays mediated by the $b \to c \ell^- \bar{\nu}_\ell$ (with $\ell = e, \mu, \tau$) transition have shown intriguing deviations from Standard Model (SM) predictions, particularly in the ratios

$$\mathcal{R}(D^{(*)}) = \frac{\mathcal{B}(B \to D^{(*)} \tau \bar{\nu}_\tau)}{\mathcal{B}(B \to D^{(*)} \mu \bar{\nu}_\mu)}. \tag{1}$$

By combining the measurements for both D and D^* final states, the observed deviation from the SM expectation reaches 3.14σ [1]. Precise determination of hadronic matrix elements is essential for accurate predictions of these ratios. In particular, an improved understanding of the $B \to D^{(*)}$ form factors is critical, as they are a major source of the theoretical uncertainties in the SM prediction of $B \to D^{(*)} \ell \bar{\nu}_\ell$. Moreover, these matrix elements are also central to resolving the tension between inclusive and exclusive determinations of the Cabibbo-Kobayashi-Maskawa (CKM) matrix element $|V_{cb}|$ [2]. The observed anomalies have motivated extensive exploration of new physics (NP) beyond the SM, including scenarios involving TeV-scale leptoquarks, exotic gauge bosons, and high-p_T searches at the LHC for potential mediator particles. Further discussions on these topics can be found in the recent comprehensive reviews [3,4].

The baryonic decay $\Lambda_b \to \Lambda_c \ell^- \bar{\nu}_\ell$ offers complementary insight into the determination of the CKM matrix element $|V_{cb}|$, which can be extracted from measurements of the differential and total decay rates in $\Lambda_b \to \Lambda_c e^-(\mu^-) \bar{\nu}_\ell$ transitions. Analogous to the ratios defined in $B \to D^{(*)} \ell \bar{\nu}_\ell$ decays, the observable

$$\mathcal{R}_{\Lambda_c} = \frac{\mathcal{B}(\Lambda_b \to \Lambda_c \tau \bar{\nu}_\tau)}{\mathcal{B}(\Lambda_b \to \Lambda_c \mu \bar{\nu}_\mu)} \tag{2}$$

can be defined, which is particularly sensitive to contributions from physics beyond the SM. The LHCb Collaboration has produced a substantial sample of Λ_b baryons, enabling precise studies of their semileptonic decays. Notably, LHCb has already reported a measurement of the semitauonic branching fraction and the ratio $\mathcal{R}_{\Lambda_c}$, as presented in Ref. [5]. With further data expected from upcoming runs, a more detailed investigation becomes both timely and promising. In this context, a comprehensive analysis of $\Lambda_b \to \Lambda_c \ell^- \bar{\nu}_\ell$ decays within the SM is warranted. In addition to $\mathcal{R}_{\Lambda_c}$, a variety of observables can be constructed, many of which exhibit enhanced sensitivity to NP effects. Precise SM predictions for these observables are therefore essential, as they provide a critical baseline for identifying and distinguishing possible deviations induced by different NP scenarios.

The semileptonic decay $\Lambda_b \to \Lambda_c \ell^- \bar{\nu}_\ell$ has attracted significant theoretical interest as a complementary channel to mesonic $b \to c \ell \bar{\nu}$ transitions. Within the SM, early

*Contact author: liying@ytu.edu.cn
†Contact author: zouzt@ytu.edu.cn

Published by the American Physical Society under the terms of the Creative Commons Attribution 4.0 International license. Further distribution of this work must maintain attribution to the author(s) and the published article's title, journal citation, and DOI. Funded by SCOAP³.

studies employed quark models and heavy-quark effective theory (HQET), while recent lattice QCD calculations have provided high-precision predictions for the full set of form factors across the kinematic range. In particular, Detmold, Lehner, and Meinel [6] calculated the $\Lambda_b \to \Lambda_c$ form factors with percentage-level uncertainties, enabling a robust extraction of $|V_{cb}|$ and predictions for observables such as $\mathcal{R}_{\Lambda_c}$. HQET-based analyses incorporating LHCb and lattice inputs have further constrained subleading corrections [7], enhancing the reliability of SM predictions. Complementary approaches, such as light cone sum rules [8], also yield results consistent with lattice data. Theoretical predictions for $\mathcal{R}_{\Lambda_c}$ in the SM lie around 0.33–0.34, in mild tension with recent LHCb measurements [5], motivating studies of possible NP effects. Global analyses have explored various NP scenarios using model-independent effective field theory frameworks [9,10], with scalar and tensor operators showing potential to accommodate observed deviations. More recently, angular analyses of the full decay chain $\Lambda_b \to \Lambda_c(\to \Lambda\pi)\tau\bar{\nu}_\tau$ have been performed to identify sensitive observables and constrain NP Wilson coefficients [11]. These efforts underscore the importance of Λ_b decays as a testing ground for LFU and as a probe of beyond-the-SM interactions. Continued theoretical refinement and forthcoming experimental data will be essential for resolving current tensions and exploring the full potential of baryonic semileptonic decays.

While lattice QCD provides precise form factor predictions in the high-q^2 (low recoil) region, its reliability decreases in the low-q^2 domain due to discretization and finite-volume effects. On the other hand, the perturbative QCD (pQCD) approach based on k_T factorization is well suited for describing heavy-to-heavy transitions in the large recoil region, where the hard-scattering kernel can be systematically expanded in α_s and nonperturbative effects are encoded in universal hadron light cone distribution amplitudes (LCDAs) [12–14]. This framework has been successfully applied to various B meson decays and extended to baryonic transitions, such as $\Lambda_b \to p$ [15,16], $\Lambda_b \to \Lambda$ [17], $\Lambda_b \to \Lambda_c$ [18–21], and $\Xi_b \to \Xi_c$ [22]. By calculating the transition form factors within the pQCD approach, one can cross check and extend lattice QCD results to the low-q^2 region, thus providing a more complete description across the entire kinematic range. Furthermore, the k_T factorization formalism includes transverse momentum effects and Sudakov suppression, which regulate endpoint divergences and enhance the theoretical control over power corrections [23,24]. A consistent treatment of Λ_b and Λ_c baryon distribution amplitudes, constrained by heavy quark symmetry and QCD sum rules [25–28], enables reliable numerical predictions. In this work, we shall revisit the $\Lambda_b \to \Lambda_c$ form factors using the pQCD framework, aiming to complement the latest lattice QCD results and to provide robust predictions for observables sensitive to new physics across the full kinematic region accessible to current and future experiments.

The content of this paper is as follows. Section II is the kinematics and the framework of the pQCD approach used in the calculation of $\Lambda_b \to \Lambda_c$ transition form factors. Section III includes wave functions of Λ_b and the Λ_c baryons. We give the results of $\Lambda_b \to \Lambda_c$ transition form factors in Sec. IV, and the $\Lambda_b \to \Lambda_c \ell^- \bar{\nu}_\ell$ decays in Sec. V, respectively. Finally, we have concluded in Sec. VI.

II. FRAMEWORK

It is convenient to adopt the light cone coordinate system, in which a four momentum is written as $p = (p^+, p^-, \mathbf{p}_T)$, with light cone components defined by $p^\pm = \frac{1}{\sqrt{2}}(p^0 \pm p^3)$ and $\mathbf{p}_T = (p^1, p^2)$. The scalar product of two arbitrary four vectors A and B is then expressed as $A \cdot B = A_\mu B^\mu = A^+B^- + A^-B^+ - \mathbf{A}_T \cdot \mathbf{B}_T$. For simplicity, we consider the Λ_b baryon at rest. We further assume that the final-state Λ_c baryon carries a large momentum component along the "$-$" light cone direction. Under these conventions, the momenta of the Λ_b and Λ_c baryons are given by

$$p = \frac{m_{\Lambda_b}}{\sqrt{2}}(1, 1, \mathbf{0}_T), \qquad p' = \frac{m_{\Lambda_b}}{\sqrt{2}}(\eta_1, \eta_2, \mathbf{0}_T). \tag{3}$$

Two components, η_1 and η_2, of p' are obtained as

$$\eta_1 = \frac{E - \sqrt{E^2 - 4m_{\Lambda_b}^2 m_{\Lambda_c}^2}}{2m_{\Lambda_b}^2},$$
$$\eta_2 = \frac{E + \sqrt{E^2 - 4m_{\Lambda_b}^2 m_{\Lambda_c}^2}}{2m_{\Lambda_b}^2}, \tag{4}$$

where $E = m_{\Lambda_b}^2 + m_{\Lambda_c}^2 - q^2$ and $q^2 = (p - p')^2 = m_{\Lambda_b}^2(1 - \eta_1)(1 - \eta_2)$. Here, m_{Λ_b} and m_{Λ_c} denote the masses of the Λ_b and Λ_c baryons, respectively. It is evident that η_2 is of order unity, $\eta_2 \sim \mathcal{O}(1)$, while η_1 is suppressed as $\eta_1 \sim \mathcal{O}(m_{\Lambda_c}^2/m_{\Lambda_b}^2)$. In the heavy quark limit, the mass difference between the b quark and the Λ_b baryon is negligible; thus, we take $m_b \simeq m_{\Lambda_b}$. The masses of the light quarks (u, d, and s) are also neglected in this approximation.

In the framework of pQCD, all transverse momenta of the valence quarks are retained. The momenta of the constituent quarks are then assigned as

$$k_1 = \left(x_1 \frac{m_{\Lambda_b}}{\sqrt{2}}, \frac{m_{\Lambda_b}}{\sqrt{2}}, \mathbf{k}_{1T}\right), \quad k_1' = \left(\frac{m_{\Lambda_b}}{\sqrt{2}}\eta_1, x_1' \frac{M}{\sqrt{2}}\eta_2, \mathbf{k}_{1T}'\right),$$
$$k_2 = \left(x_2 \frac{m_{\Lambda_b}}{\sqrt{2}}, 0, \mathbf{k}_{2T}\right), \quad k_2' = \left(0, x_2' \frac{m_{\Lambda_b}}{\sqrt{2}}\eta_2, \mathbf{k}_{2T}'\right),$$
$$k_3 = \left(x_3 \frac{m_{\Lambda_b}}{\sqrt{2}}, 0, \mathbf{k}_{3T}\right), \quad k_3' = \left(0, x_3' \frac{m_{\Lambda_b}}{\sqrt{2}}\eta_2, \mathbf{k}_{3T}'\right). \tag{5}$$

Here, the b and c quarks are treated as massive and carry momenta k_1 and k_1', respectively. The momenta $k_2(k_3)$ and k_2' (k_3') correspond to the spectator u (d) quarks in the Λ_b and Λ_c baryons, respectively. The x_i and x_i' denote the longitudinal momentum fractions of the valence quarks, and $\mathbf{k}_{iT}, \mathbf{k}_{iT}'$ represent their transverse momenta. These momenta satisfy the following conservation relations:

$$x_1 + x_2 + x_3 = 1, \qquad \mathbf{k}_{1T} + \mathbf{k}_{2T} + \mathbf{k}_{3T} = 0, \quad (6)$$

and the same conditions hold for the primed quantities.

Factorization is a central concept in applying pQCD to hard exclusive processes, as it allows the separation of long-distance (nonperturbative) dynamics from short-distance (perturbative) dynamics. The hadronic matrix elements for the $\Lambda_b \to \Lambda_c$ transition can be expressed as

$$\mathcal{M} \sim \Psi_{\Lambda_b}(x_i, b_i, \mu) \otimes H(x_i, b_i, x_i', b_i', \mu) \otimes \Psi_{\Lambda_c}(x_i', b_i', \mu), \quad (7)$$

where H denotes the hard scattering kernel, and Ψ_{Λ_b} and Ψ_{Λ_c} are the wave functions of the Λ_b and Λ_c baryons, respectively. Both the wave functions and the hard kernel H depend on the factorization scale μ, which serves as the boundary separating soft and hard dynamics. Above this scale, the dynamics are governed by perturbative (short-distance) interactions; below it, the dynamics are nonperturbative and are absorbed into the hadron wave functions. The factorization scale is typically chosen to be equal to the renormalization scale for convenience. In practical calculations, it is advantageous to work in transverse coordinate space (commonly referred to as b space) rather than in transverse momentum space ($\mathbf{k}_T$ space). Accordingly, a Fourier transformation is performed to convert the wave functions and the hard amplitude into b space. The variable $1/b$ naturally emerges as a typical scale separating hard and soft regions. For scales $\mu > 1/b$, the interactions are dominated by short-distance QCD dynamics and are computed perturbatively. Conversely, for $\mu < 1/b$, soft contributions dominate and are included in the nonperturbative wave functions. This treatment ensures a consistent separation of perturbative and nonperturbative effects within the k_T factorization formalism.

Higher-order radiative corrections to both the wave functions and the hard scattering amplitudes give rise to large double logarithmic terms of the form $\alpha_s \ln^2(Qb)$, which originate from the overlap of collinear and soft divergences. To ensure the validity of the perturbative expansion, such large logarithms must be systematically resummed. Resummation techniques have been developed for this purpose, leading to the appearance of a Sudakov exponential factor, $\exp[-s(Q,b)]$, which suppresses contributions from large transverse separations. This exponential falls rapidly with increasing b and vanishes as $b \to 1/\Lambda_{\rm QCD}$. As a result, the full hadronic wave functions $\Psi_{\Lambda_b}(x, \mathbf{b}, p, \mu)$ and $\Psi_{\Lambda_c}(x', \mathbf{b}', p', \mu)$ can be factorized into products of the Sudakov exponentials and reduced (nonperturbative) wave functions, denoted by $\Phi_{\Lambda_b}(x, \mathbf{b}, p, \mu)$ and $\Phi_{\Lambda_c}(x', \mathbf{b}', p', \mu)$:

$$\Psi_{\Lambda_b}(x, \mathbf{b}, p, \mu) = \exp\left[-\sum_{i=2}^{3} s(w, k_i^+)\right] \Phi_{\Lambda_b}(x, \mathbf{b}, p, \mu), \quad (8)$$

$$\Psi_{\Lambda_c}(x', \mathbf{b}', p', \mu) = \exp\left[-\sum_{i=1}^{3} s(w', k_i'^-)\right] \Phi_{\Lambda_c}(x', \mathbf{b}', p', \mu), \quad (9)$$

where the expressions of k_i^+ and $k_i'^-$ are presented in Eq. (5). The Sudakov exponent function $s(w, Q)$ is given by [29]

$$s(w, Q) = \int_w^Q \frac{dp}{p}\left[\ln\left(\frac{Q}{p}\right) A(\alpha_s(p)) + B(\alpha_s(p))\right], \quad (10)$$

where the anomalous dimensions A to two loops and B to one loop are

$$A = C_F \frac{\alpha_s}{\pi} + \left[\frac{67}{9} - \frac{\pi^2}{3} - \frac{10}{27} n_f + \frac{8}{3}\beta_0 \ln\left(\frac{e^{\gamma_E}}{2}\right)\right]\left(\frac{\alpha_s}{\pi}\right)^2, \quad (11)$$

$$B = \frac{2}{3}\frac{\alpha_s}{\pi} \ln\left(\frac{e^{2\gamma_E - 1}}{2}\right), \quad (12)$$

$n_f = 4$ for Λ_b baryon decays being the flavor number, and γ_E the Euler constant. The two-loop running coupling constant,

$$\frac{\alpha_s(\mu)}{\pi} = \frac{1}{\beta_0 \ln(\mu^2/\Lambda^2)} - \frac{\beta_1}{\beta_0^3} \frac{\ln\ln(\mu^2/\Lambda^2)}{\ln^2(\mu^2/\Lambda^2)}, \quad (13)$$

with the coefficients

$$\beta_0 = \frac{33 - 2n_f}{12}, \qquad \beta_1 = \frac{153 - 19 n_f}{24}, \quad (14)$$

and the QCD scale $\Lambda \equiv \Lambda_{\rm QCD}$, will be substituted into Eq. (10). The factorization scales w and w' characterize the inverse of typical transverse separations among the three valence quarks in the initial and final baryons, respectively, and are defined as

$$w = \min\left(\frac{1}{b_1}, \frac{1}{b_2}, \frac{1}{b_3}\right), \qquad w' = \min\left(\frac{1}{b_1'}, \frac{1}{b_2'}, \frac{1}{b_3'}\right), \quad (15)$$

where

$$b_1 = |\mathbf{b}_2 - \mathbf{b}_3|, \qquad b_1' = |\mathbf{b}_2' - \mathbf{b}_3'|, \tag{16}$$

and the remaining b_i and b_i' are obtained by cyclic permutations.

Apart from the double logarithms arising from the inclusion of transverse momentum, large single logarithms originating from ultraviolet divergences also appear in the radiative corrections to both the hadronic wave functions and the hard kernels. These single logarithms can be resummed using the renormalization group (RG) method. As a result, we obtain

$$\begin{aligned}
\Phi_{\Lambda_b}(x,\mathbf{b},p,\mu) &= \exp\left[-\frac{8}{3}\int_{\kappa w}^{\mu}\frac{d\bar{\mu}}{\bar{\mu}}\gamma_q(\alpha_s(\bar{\mu}))\right] \\
&\quad\times \Phi_{\Lambda_b}(x,\mathbf{b},p,w), \\
\Phi_{\Lambda_c}(x',\mathbf{b}',p',\mu) &= \exp\left[-3\int_{\kappa w'}^{\mu}\frac{d\bar{\mu}}{\bar{\mu}}\gamma_q(\alpha_s(\bar{\mu}))\right] \\
&\quad\times \Phi_{\Lambda_c}(x',\mathbf{b}',p',w'), \\
H(x,x',\mathbf{b},\mathbf{b}',\mu) &= \exp\left[-\frac{17}{3}\int_{\mu}^{t}\frac{d\bar{\mu}}{\bar{\mu}}\gamma_q(\alpha_s(\bar{\mu}))\right] \\
&\quad\times H(x,x',\mathbf{b},\mathbf{b}',t),
\end{aligned} \tag{17}$$

where the quark anomalous dimension in the axial gauge is given by $\gamma_q = -\alpha_s/\pi$. The parameter κ is introduced to characterize different schemes for distributing radiative corrections between the perturbative Sudakov factor and the nonperturbative wave function. The value $\kappa = 1.14$ is adopted following the fit to the proton form factor [30].

It should be noted that radiative corrections to the hard amplitudes can generate large double logarithms of the form $\alpha_s \ln^2 x$, which must also be resummed to all orders. The resulting threshold resummation function $S_t(x)$ vanishes rapidly in the end-point regions, $x \to 0$ and $x \to 1$, thereby suppressing contributions from these regions in processes such as B meson decays to light mesons, such as $B \to \pi$ and $B \to K$ processes [31]. In contrast, this suppression is less significant in $B \to D$ transitions [32]. Since the $\Lambda_b \to \Lambda_c$ transition also falls into the category of heavy-to-heavy processes, we adopt the simplification $S_t(x) = 1$ in our analysis. We also note that the systematic derivation of $S_t(x)$ for baryonic decays is beyond the scope of this work, and we will explore it in the future.

Finally, the matrix element for the $\Lambda_b \to \Lambda_c$ transition can be expressed as

$$\begin{aligned}
\mathcal{M} \sim \Phi_{\Lambda_b}(x_i,b_i,\omega) \otimes H(x_i,b_i,x_i',b_i',t) \otimes \Phi_{\Lambda_c}(x_i',b_i',\omega') \\
\otimes \exp[-S],
\end{aligned} \tag{18}$$

where the explicit form of the Sudakov factor S is given by [19]

$$\begin{aligned}
S = &\sum_{l=2,3} s(w,k_l^+) + \sum_{l=1,2,3} s(w',k_l'^-) \\
&+ \frac{8}{3}\int_{\kappa w}^{t}\frac{d\bar{\mu}}{\bar{\mu}}\gamma_q(\alpha_s(\bar{\mu})) + 3\int_{\kappa w'}^{t}\frac{d\bar{\mu}}{\bar{\mu}}\gamma_q(\alpha_s(\bar{\mu})).
\end{aligned} \tag{19}$$

III. THE WAVE FUNCTIONS

The wave functions of both the initial and final states are among the most crucial input parameters in the pQCD approach. Both the Λ_b and Λ_c baryons are composed of a heavy quark and two light quarks. In the heavy quark limit, the dynamics of the heavy quark can be factorized from the light degrees of freedom. Assuming that the orbital and spin degrees of freedom of the light-quark system decouple, the distribution amplitude (LCDA) of the Λ_b baryon can be written as [33]

$$\begin{aligned}
\Phi_{\Lambda_b,\alpha\beta\gamma} &= \frac{1}{2\sqrt{2}N_c}\int\prod_{l=2}^{3}\frac{dy_l^- d\mathbf{y}_l}{(2\pi)^3}e^{ik_l\cdot y_l}\epsilon^{abc}\langle 0|T[b_\alpha^a(y_1)u_\beta^b(y_2)d_\gamma^c(0)]|u_{\Lambda_b}(p,s)\rangle \\
&= \frac{f_{\Lambda_b}}{8\sqrt{2}N_c}[(\not{p}+m_{\Lambda_b})\gamma_5 C]_{\beta\gamma}[u_{\Lambda_b}(p,s)]_\alpha\phi_{\Lambda_b}(k_i,\mu),
\end{aligned} \tag{20}$$

where u_{Λ_b} denotes the heavy baryon spinor; a, b, and c are color indices; and α, β, and γ are spinor indices. N_c is the number of colors, and C is the charge conjugation matrix. The parameter $f_{\Lambda_b} = 2.71 \times 10^{-3}$ GeV^2 [18] is the normalization constant. Under similar assumptions, the distribution amplitude of the Λ_c baryon, $\Phi_{\Lambda_c,\alpha'\beta'\gamma'}$, can be written as

$$\begin{aligned}
\Phi_{\Lambda_c,\alpha'\beta'\gamma'} &= \frac{1}{2\sqrt{2}N_c}\int\prod_{l=2}^{3}\frac{dy_l' d\mathbf{y}_l'}{(2\pi)^3}e^{ik_l'\cdot y_l'}\epsilon^{abc}\langle 0|T[c_{\alpha'}^a(y_1')u_{\beta'}^b(y_2')d_{\gamma'}^c(0)]|u_{\Lambda_c}(p',s')\rangle \\
&= \frac{f_{\Lambda_c}}{8\sqrt{2}N_c}[(\not{p}'+m_{\Lambda_c})\gamma_5 C]_{\beta'\gamma'}[u_{\Lambda_c}(p',s')]_{\alpha'}\phi_{\Lambda_c}(k_i',\mu).
\end{aligned} \tag{21}$$

In the heavy quark limit, the approximate relation $f_{\Lambda_b}m_{\Lambda_b} = f_{\Lambda_c}m_{\Lambda_c}$ [18] is satisfied. Therefore, we take $f_{\Lambda_c} = 6.66 \times 10^{-3}$ GeV^2.

The phenomenological model for the distribution amplitude of the Λ_b baryon employed in this work is given by [34]

$$\phi_{\Lambda_b}(x_1, x_2, x_3) = N_{\Lambda_b} x_1 x_2 x_3 \exp\left[-\frac{1}{2\beta_b^2}\left(\frac{m_b^2}{x_1} + \frac{m_u^2}{x_2} + \frac{m_d^2}{x_3}\right)\right], \quad (22)$$

where β_b is the shape parameter and m_q $(q = u,\ d,\ b)$ denotes the masses of the constituent quarks in the baryon. The normalization constant N_{Λ_b} is determined by

$$\int dx_1 dx_2 dx_3 \delta(x_1 + x_2 + x_3 - 1)\phi_{\Lambda_b}(x_1, x_2, x_3) = 1. \quad (23)$$

It is evident that the function $\phi_{\Lambda_b}(x_1, x_2, x_3)$ is symmetric under the exchange of the two light quarks. For the LCDA of the Λ_c baryon, we adopt the same form, since the masses of the bottom and charm quarks are both significantly larger than those of the light quarks. The above forms have been adopted in various phenomenological studies [18,20,35].

Recent developments have significantly advanced our understanding of the LCDAs of heavy baryons Λ_b and Λ_c. At leading twist, the Λ_b LCDA has been studied within the framework of HQET, under the assumption that the light diquark system forms a spin-zero configuration. The RG evolution of the leading-twist LCDA has been derived using light cone operator techniques [36,37]. Higher-twist three-quark LCDAs have also been systematically classified and evaluated via QCD sum rules [26,38], revealing that the distributions are sharply peaked when the heavy quark carries the majority of the baryon's momentum. Similar studies have been extended to the Λ_c system under analogous assumptions [25,39], indicating that pQCD factorization can remain valid in specific heavy-to-heavy kinematic regimes. Recent progress also includes next-to-leading-order corrections to the evolution equations and normalization conditions, which have improved the theoretical precision of these frameworks. Concurrently, lattice QCD has begun providing first-principles estimates for low-order moments of the Λ_b LCDA [40,41], offering increasingly stringent constraints on phenomenological models. However, as the precision of LCDA determinations improves, the introduction of additional shape parameters can paradoxically amplify theoretical uncertainties. To avoid this, we still adopt the form in Eq. (22), which uses the minimal number of parameters required to capture the essential features of the distribution.

IV. $\Lambda_b \to \Lambda_c$ FORM FACTORS

The $\Lambda_b \to \Lambda_c$ transition matrix elements induced by the vector and axial-vector currents can be decomposed into three dimensionless invariant form factors [42,43]:

$$\langle \Lambda_c(p', s')|\bar{c}\gamma^\mu b|\Lambda_b(p, s)\rangle = \bar{u}_{\Lambda_c}(p', s')\left[f_1(q^2)\gamma^\mu - \frac{f_2(q^2)}{m_{\Lambda_b}} i\sigma^{\mu\nu} q_\nu + \frac{f_3(q^2)}{m_{\Lambda_b}} q^\mu\right] u_{\Lambda_b}(p, s), \quad (24)$$

$$\langle \Lambda_c(p', s')|\bar{c}\gamma^\mu\gamma_5 b|\Lambda_b(p, s)\rangle = \bar{u}_{\Lambda_c}(p', s')\left[g_1(q^2)\gamma^\mu - \frac{g_2(q^2)}{m_{\Lambda_b}} i\sigma^{\mu\nu} q_\nu + \frac{g_3(q^2)}{m_{\Lambda_b}} q^\mu\right]\gamma_5 u_{\Lambda_b}(p, s), \quad (25)$$

where $\sigma^{\mu\nu} = i(\gamma^\mu\gamma^\nu - \gamma^\nu\gamma^\mu)/2$, and the four-momentum transfer q is constrained by the physical kinematic region $0 < q^2 < (m_{\Lambda_b} - m_{\Lambda_c})^2$.

In the previous section, we discussed the wave functions appearing in the factorization formula in Eq. (18). In this section, we calculate the hard part H, which includes the current operators and the necessary hard gluon exchanges connecting the current to the spectator quarks. Since the final results are expressed as integrals over the distribution variables, we present the full amplitude for each diagram, incorporating the wave functions and Sudakov factors. Given that the pQCD predictions are most reliable in the large recoil (small q^2) region, we evaluate the form factors at $q^2 = 0$ and subsequently extrapolate them over the entire kinematic range, $0 \le q^2 \le (m_{\Lambda_b} - m_{\Lambda_c})^2$, so as to estimate the branching fractions of the semileptonic decays $\Lambda_b \to \Lambda_c \ell^- \bar{\nu}_\ell$.

In the conventional quark model, a baryon consists of three constituent quarks, making the QCD dynamics of baryon decay processes inherently more complicated than those of mesons. This complexity arises from the increased number of possible gluon exchanges, particularly within the pQCD framework, where at least two hard gluon exchanges are required at leading-order approximation. Consequently, the decay amplitudes for processes such as $\Lambda_b \to \Lambda_c$ begin at the order of $\mathcal{O}(\alpha_s^2)$ in pQCD. All factorizable Feynman diagrams contributing to this decay are illustrated in Fig. 1.

It is noteworthy that several diagrams in Fig. 1 are related through the interchange of two light quarks. For instance, diagram T_1 can be transformed into T_{11} by exchanging the up and down quarks ($u \leftrightarrow d$). As a result, the amplitude of T_{11} can be obtained from that of T_1 by simultaneously swapping the momentum indices 2 and 3 and the spinor

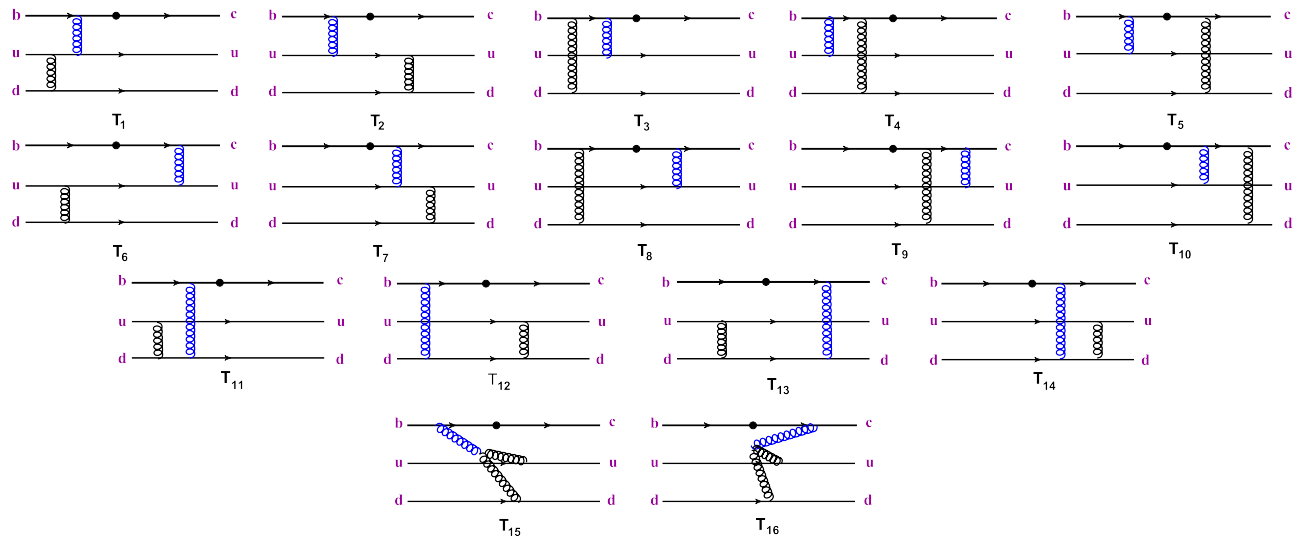


FIG. 1. Feynman diagrams for the $\Lambda_b \to \Lambda_c$ transition form factors with T_i. These diagrams are marked in sequence as $T_1, T_2, \ldots$ and T_{16} in this work.

indices β and γ. In contrast, diagrams (T_{15} and T_{16}) involving the triple-gluon vertex do not contribute in this analysis, as their corresponding color factors vanish in the present case. Based on this symmetry, the following pairs of diagrams are found to be equivalent:

$$T_1 = T_{11}, \qquad T_2 = T_{12}, \qquad T_3 = T_4, \qquad T_5 = T_8,$$
$$T_6 = T_{13}, \qquad T_7 = T_{14}, \qquad T_9 = T_{10}. \tag{26}$$

So, we only need to calculate the seven left diagrams, T_1, T_2, T_3, T_5, T_6, T_7, and T_9.

For each diagram T_i, the contribution of diagram to the form factor F_j ($F = f,\ g$) can be evaluated at $q^2 = 0$, yielding

$$F_j^{T_i}(q^2 = 0) = \mathcal{C}\frac{f_{\Lambda_b} f_{\Lambda_c} \pi^3}{4N_c^2} \int [\mathcal{D}x] \int [\mathcal{D}b] \int [\mathcal{D}\theta] \times \phi_{\Lambda_b} \phi_{\Lambda_c} \alpha_s^2(t_{T_i}) B_{T_i} H_{F_j}^{T_i} \exp[-S_{T_i}], \tag{27}$$

where $\mathcal{C} = 8/3$ is the color factor. The integration measure over the momentum fractions is defined as

$$[\mathcal{D}x] = [dx][dx'], \tag{28}$$

$$[dx] = dx_1 dx_2 dx_3 \delta(1 - x_1 - x_2 - x_3), \tag{29}$$

$$[dx'] = dx'_1 dx'_2 dx'_3 \delta(1 - x'_1 - x'_2 - x'_3), \tag{30}$$

while the measure for the transverse separations reads as

$$[\mathcal{D}b] = b_2 b_3 b'_2 b'_3 db_2 db_3 db'_2 db'_3, \tag{31}$$

and the angular integration over the relative orientations in transverse (b-)space is given by

$$[\mathcal{D}\theta] = d\theta_1 d\theta_2 d\theta_3. \tag{32}$$

The hard function B_{T_i} originates from the Fourier transformation of denominators of the internal propagators in diagram T_i, while $H_{F_j}^{T_i}$ denotes the hard scattering amplitude, which depends on the spinor structures of the valence quarks in the initial and final baryons. Explicit expressions for both B_{T_j} and H^{T_j} are provided in the Appendix. Following the same procedure, we calculate all form factor components $f_i^{T_j}$ and $g_i^{T_j}$ for each contributing diagram. The complete analytic expressions are also collected in the Appendix. Finally, summing over all diagrams yields the full form factors f_i and g_i at $q^2 = 0$.

The numerical results for the form factors are summarized in Table I, alongside those obtained from various theoretical approaches in the literature for comparison. The dominant theoretical uncertainties arise from the shape parameters β_Q in the baryon LCDAs, the charm quark mass m_c, and the choice of the hard scale t. In our analysis, we estimate these uncertainties by varying β_Q and m_c within a 10% range, and by varying the hard scale in the range $0.8t$ to $1.2t$. Among these sources, the most significant uncertainty originates from the baryon LCDAs, contributing up to 23% in magnitude. This sizable uncertainty highlights the necessity of better constraining the nonperturbative parameters in the baryon distribution amplitudes to improve the precision of theoretical predictions.

In order to calculate the observables of semileptonic decays $\Lambda_b \to \Lambda_c \ell^- \bar{\nu}_\ell$ ($\ell = e,\ \mu,\ \tau$), the behaviors of the form factors in the whole kinematic range $0 \le q^2 \le (m_{\Lambda_b} - m_{\Lambda_c})^2$ are required. Now, we shall extrapolate from the low q^2 to the higher q^2 region for all form factors. In the literature, there are lots of parameterizations, such as the single-pole model and double pole model. In this work,

TABLE I. Results of the form factor at $q^2 = 0$ of this work are compared with those of other methods.

	$f_1(0)$	$f_2(0)$	$f_3(0)$	$g_1(0)$	$g_2(0)$	$g_3(0)$
This work	$0.499^{+0.091}_{-0.110}$	$0.085^{+0.026}_{-0.027}$	$-0.086^{+0.029}_{-0.022}$	$0.504^{+0.076}_{-0.119}$	$0.091^{+0.027}_{-0.030}$	$-0.088^{+0.030}_{-0.020}$
LCSR [28]	0.583	0.144	−0.115	0.583	0.114	−0.115
QCDSR [44]	0.467	0.123	0.022	0.434	−0.036	−0.160
LFQM [45]	0.500	0.098	−0.009	0.509	0.015	−0.085
LFQM [39]	0.50 ± 0.05	0.12 ± 0.01	-0.04 ± 0.00	0.49 ± 0.05	0.02 ± 0.00	-0.15 ± 0.02
RQM [46]	0.526	0.136	0.075	0.504	−0.026	−0.251
CCQM [43]	0.549	0.110	−0.023	0.542	0.018	−0.123
LQCD [6]	0.418	0.091	−0.075	0.378	0.104	−0.105
LFQM [47]	0.506	0.099	⋯	0.501	0.008	⋯
LFQM [48]	0.670	0.132	⋯	0.656	0.012	⋯
LFQM [49]	$0.474^{+0.069}_{-0.072}$	$0.108^{+0.020}_{-0.019}$	$0.049^{+0.014}_{-0.015}$	$0.468^{+0.067}_{-0.070}$	$-0.050^{+0.011}_{-0.008}$	$-0.118^{+0.017}_{-0.015}$
LFQM [50]	0.488	0.180	⋯	0.470	0.048	⋯
pQCD [21]	$0.440^{+0.136}_{-0.173}$	⋯	⋯	$0.443^{+0.143}_{-0.181}$	⋯	⋯

we shall adopt the simplified z-series parametrization [28]

$$f_i(q^2) = \frac{f_i(0)}{1 - q^2/m^2_{B_c^*(1^-)}}\{1 + a_1[z(q^2,0) - z(0,t_0)]\},$$
$$g_i(q^2) = \frac{g_i(0)}{1 - q^2/m^2_{B_c^*(1^+)}}\{1 + b_1[z(q^2,0) - z(0,t_0)]\}, \tag{33}$$

where the parameter z is defined as

$$z(q^2,t_0) = \frac{\sqrt{t_+ - q^2} - \sqrt{t_+ - t_0}}{\sqrt{t_+ - q^2} + \sqrt{t_+ - t_0}} \tag{34}$$

with $t_\pm = (m_{\Lambda_b} \pm m_{\Lambda_c})^2$ and $t_0 = t_+(1 - \sqrt{1 - t_-/t_+})$. The masses of $B_c^*(1^-)$ and $B_c^*(1^+)$ appear in the pole factor but are not measured. There are several theoretical estimations of these masses, and we adopt $m_{B^*(1^-)} = 6.336$ GeV and $m_{B^*(1^+)} = 6.745$ GeV [7].

It is known to us that the form factors based on pQCD are reliable only in the low q^2 region, and in the large q^2 region, the applicability of the pQCD framework may break down. In addition, we also know that in the large q^2 region, the results based on the lattice QCD are reliable. In Ref. [6], the lattice QCD results for the six form factors are published, from which we obtain the numerical results at $q^2_{\rm max} = (m_{\Lambda_b} - m_{\Lambda_c})^2$ as

$$f_1(q^2_{\rm max}) = 1.025, \quad g_1(q^2_{\rm max}) = 0.928,$$
$$f_2(q^2_{\rm max}) = 0.208, \quad g_2(q^2_{\rm max}) = 0.234,$$
$$f_3(q^2_{\rm max}) = -0.211, \quad g_3(q^2_{\rm max}) = -0.207. \tag{35}$$

Thus, in the low q^2 region from 0 to m_τ^2, m_τ being the τ lepton mass, we adopt results of pQCD approach, while in the large q^2 region, we use the results from lattice QCD, as shown in Eq. (35). Within the data, the fitted results of a_1, b_1 are presented in Table II. The fitted q^2 behaviors of the form factors (red solid lines) in the allowed region are also illustrated in Fig. 2, and the uncertainties are only from pQCD calculations. As is expected from weak decays, the form factors demonstrate a good behavior that their magnitudes grow gradually with increasing q^2. $f_1(q^2)$ and $g_1(q^2)$ show similar q^2 dependence and dominate over other four form factors. For comparison, we also present the extrapolated curves (blue dashed) obtained from lattice calculations, which extends the lattice results from large q^2 down to low q^2, in contrast to the present analysis that proceeds from low to large q^2. It is obvious that for $f_1(0)$ and $g_1(0)$, our results are larger than that extrapolated with lattice data.

TABLE II. Fitted result of a_1, b_1 for the form factors.

F	$F(0)$	a_1	b_1
f_1	$0.499^{+0.091}_{-0.110}$	$-9.73^{+1.98}_{-2.32}$	
f_2	$0.083^{+0.026}_{-0.027}$	$-17.37^{+3.75}_{-5.21}$	
f_3	$-0.086^{+0.029}_{-0.022}$	$-15.96^{+5.04}_{-5.49}$	
g_1	$0.504^{+0.076}_{-0.119}$		$-8.34^{+1.83}_{-3.28}$
g_2	$0.091^{+0.027}_{-0.030}$		$-18.91^{+5.49}_{-6.09}$
g_3	$-0.088^{+0.030}_{-0.020}$		$-16.35^{+4.61}_{-5.37}$

V. ANALYSIS OF $\Lambda_b \to \Lambda_c \ell^- \bar{\nu}_\ell$

In this section, we shall explore the phenomenological applications of the obtained $\Lambda_b \to \Lambda_c$ form factors, which serve as essential inputs for the theoretical description of the semileptonic decay $\Lambda_b \to \Lambda_c \ell^- \bar{\nu}_\ell$. Within the SM, this decay is typically viewed as proceeding through an intermediate off shell W^{*-} boson: $\Lambda_b \to \Lambda_c W^{*-}$, followed by the subsequent decay $W^{*-} \to \ell^- \bar{\nu}_\ell$. The off shell W^{*-} boson can carry four helicity states: $\lambda_W = \pm 1, 0$ (with total spin $J = 1$), and a scalar polarization corresponding to

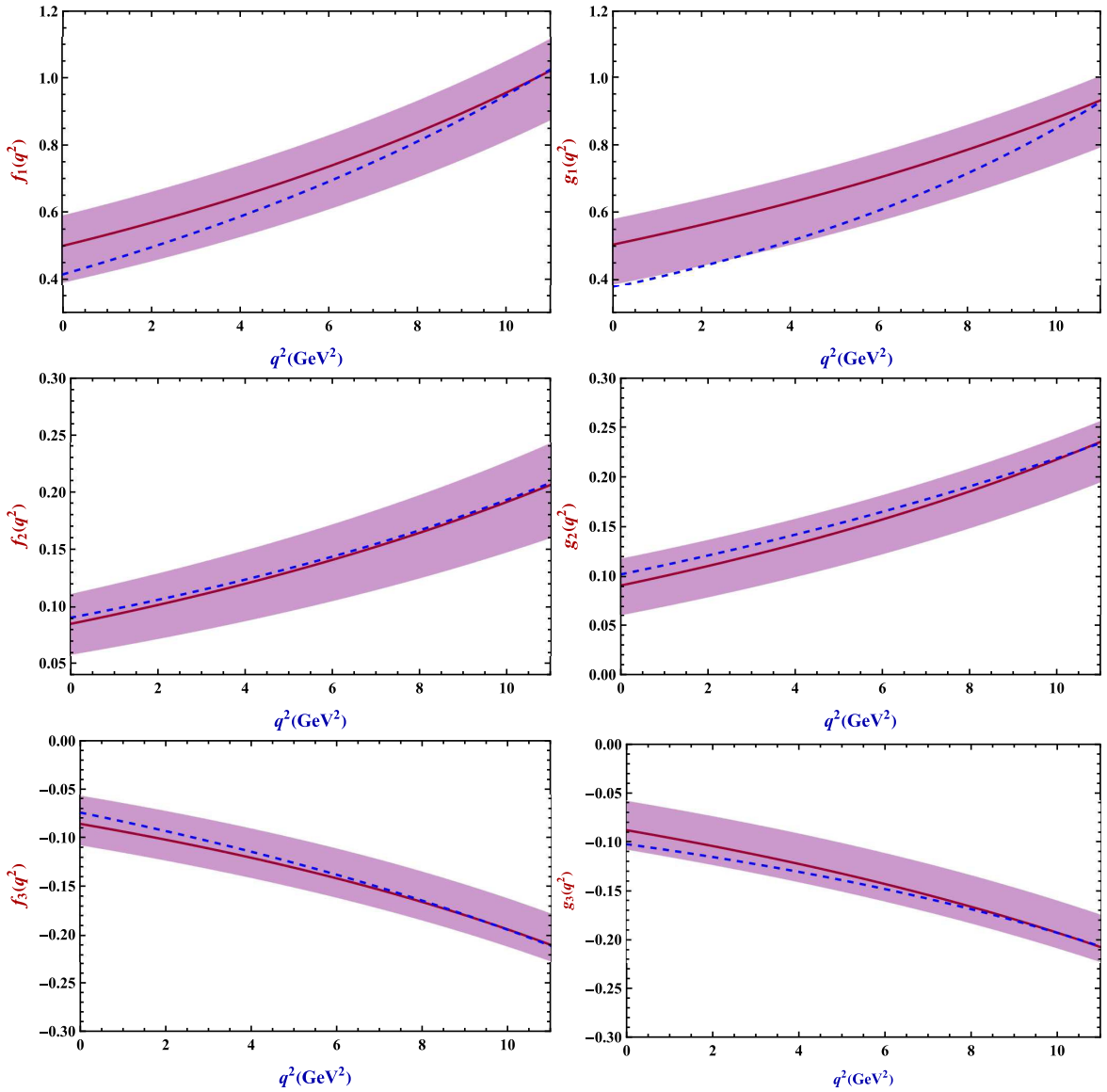


FIG. 2. The fitted q^2 dependence of the six form factors in the physical region. The red solid curves denote the fitted results obtained using pQCD inputs at low q^2 and lattice-QCD inputs at high q^2, with the bands representing the uncertainties originating solely from the PQCD calculations. For comparison, the blue dashed curves correspond to the extrapolated results from lattice calculations.

$J = 0$, also labeled by $\lambda_W = 0$. To distinguish between these two states with $\lambda_W = 0$, we adopt the notation $\lambda_W = 0$ for the longitudinal polarization ($J = 1$) and $\lambda_W = t$ for the scalar (timelike) polarization ($J = 0$).

In the rest frame of the Λ_b baryon, with the z axis defined along the momentum direction of the virtual W^{*-} boson, the polarization vectors of the W^{*-} are given by

$$\begin{aligned}\varepsilon^\mu(\pm) &= \frac{1}{\sqrt{2}}(0, 1, \mp i, 0),\\ \varepsilon^\mu(0) &= -\frac{1}{\sqrt{q^2}}(q_z, 0, 0, q_0),\\ \varepsilon^\mu(t) &= -\frac{q^\mu}{\sqrt{q^2}},\end{aligned} \tag{36}$$

where q^μ denotes the four momentum of the off shell W^{*-} boson. These polarization vectors satisfy the following orthonormality and completeness relations:

$$\varepsilon^{*\mu}(m)\epsilon_\mu(n) = g_{mn}, \qquad \sum_{m,n}\varepsilon^{*\mu}(m)\varepsilon^{\nu}(n)g_{mn} = g^{\mu\nu}, \tag{37}$$

with $g_{mn} = \mathrm{diag}(+,-,-,-)$ for $m, n = t, \pm, 0$. Because the current is not conserved in SM, it consists of a superposition of a spin-1 and a spin-0 component where the J^P content of the vector current J_μ^V and the axial vector current J_μ^A are $(0^+, 1^-)$ and $(0^-, 1^+)$, respectively.

In the calculation of the $\Lambda_b \to \Lambda_c \ell^- \bar{\nu}_\ell$ decay, the total transition matrix element can be factorized into a leptonic part and a hadronic part, each of which is not Lorentz

invariant by itself. However, upon inserting the completeness relations of the intermediate off shell W^{*-} boson, both the hadronic and leptonic contributions become Lorentz invariant. This allows us to choose the most convenient reference frames for evaluating each part of the amplitude. Specifically, the hadronic transition is analyzed in the rest frame of the initial Λ_b baryon, while the leptonic part is evaluated in the rest frame of the virtual W^{*-} boson. Based on this setup, we proceed to calculate the helicity amplitudes for the $\Lambda_b \to \Lambda_c W^{*-}$ transition as follows:

$$H^{V(A)}_{\lambda_{\Lambda_c},\lambda_W} = \varepsilon^{*\mu}(\lambda_{W^-})\langle \Lambda_c(\lambda_{\Lambda_c})|V(A)|\Lambda_b(\lambda_{\Lambda_b})\rangle, \quad (38)$$

where $\lambda_{\Lambda_b}, \lambda_{\Lambda_c}, \lambda_W$ denote the helicity of the Λ_b baryon, Λ_c baryon, and off shell W^{*-}, respectively. Owing to the conservation of angular momentum, $\lambda_1 = -\lambda_2 + \lambda_W$ is satisfied. The various helicity amplitudes are then expressed, in terms of the $\Lambda_b \to \Lambda_c$ form factors, as [43,51–56]

$$H^V_{\frac{1}{2},0} = \frac{\sqrt{(m_{\Lambda_b} - m_{\Lambda_c})^2 - q^2}}{\sqrt{q^2}} \times \left[(m_{\Lambda_b} + m_{\Lambda_c}) f_1(q^2) + \frac{q^2}{m_{\Lambda_b}} f_2(q^2)\right], \quad (39)$$

$$H^A_{\frac{1}{2},0} = \frac{\sqrt{(m_{\Lambda_b} + m_{\Lambda_c})^2 - q^2}}{\sqrt{q^2}} \times \left[(m_{\Lambda_b} - m_{\Lambda_c}) g_1(q^2) - \frac{q^2}{m_{\Lambda_b}} g_2(q^2)\right], \quad (40)$$

$$H^V_{\frac{1}{2},1} = \sqrt{2[(m_{\Lambda_b} - m_{\Lambda_c})^2 - q^2]} \times \left[-f_1(q^2) - \frac{m_{\Lambda_b} + m_{\Lambda_c}}{m_{\Lambda_b}} f_2(q^2)\right], \quad (41)$$

$$H^A_{\frac{1}{2},1} = \sqrt{2[(m_{\Lambda_b} + m_{\Lambda_c})^2 - q^2]} \times \left[-g_1(q^2) + \frac{m_{\Lambda_b} - m_{\Lambda_c}}{m_{\Lambda_b}} g_2(q^2)\right], \quad (42)$$

$$H^V_{\frac{1}{2},t} = \frac{\sqrt{(m_{\Lambda_b} + m_{\Lambda_c})^2 - q^2}}{\sqrt{q^2}} \times \left[(m_{\Lambda_b} - m_{\Lambda_c}) f_1(q^2) + \frac{q^2}{m_{\Lambda_b}} f_3(q^2)\right], \quad (43)$$

$$H^A_{\frac{1}{2},t} = \frac{\sqrt{(m_{\Lambda_b} - m_{\Lambda_c})^2 - q^2}}{\sqrt{q^2}} \times \left[(m_{\Lambda_b} + m_{\Lambda_c}) g_1(q^2) - \frac{q^2}{m_{\Lambda_b}} g_3(q^2)\right], \quad (44)$$

where the subscript t refers to the temporal component of the helicities of the off shell W^- boson [43]. The amplitudes with negative helicities can be obtained by

$$H^V_{-\lambda_{\Lambda_c},-\lambda_W} = H^V_{\lambda_{\Lambda_c},\lambda_W}, \quad H^A_{-\lambda_{\Lambda_c},-\lambda_W} = -H^A_{\lambda_{\Lambda_c},\lambda_W}. \quad (45)$$

Then, we have the helicity amplitude as

$$H_{\lambda_{\Lambda_c},\lambda_W} = H^V_{\lambda_{\Lambda_c},\lambda_W} - H^A_{\lambda_{\Lambda_c},\lambda_W}. \quad (46)$$

Since the leptonic sector is free from hadronic QCD complications, the corresponding amplitudes can be evaluated analytically. Detailed expressions are available in Ref. [57].

The differential angular distributions for the semileptonic decays $\Lambda_b \to \Lambda_c \ell^- \bar{\nu}_\ell$ are given by [28,39,51]

$$\frac{d\Gamma(\Lambda_b \to \Lambda_c \ell^- \bar{\nu}_\ell)}{dq^2 d\cos\theta_\ell} = \frac{G_F^2 |V_{cb}|^2 q^2 |\vec{p}_c|}{512\pi^3 m_{\Lambda_b}^2}\left(1 - \frac{m_\ell^2}{q^2}\right)^2 \times \left(A_1 + \frac{m_\ell^2}{q^2} A_2\right), \quad (47)$$

where m_ℓ is the lepton mass ($\ell = e, \mu, \tau$), G_F is the Fermi constant, V_{cb} is the CKM matrix element, θ_ℓ stands for the angle between the charged lepton and the final Λ_c baryon in the Λ_b baryon rest frame, and $\vec{p}_c$ is the three momentum of the Λ_c baryon. The amplitudes A_1, A_2 are defined as

$$A_1 = 2\sin^2\theta_\ell (H^2_{\frac{1}{2},0} + H^2_{-\frac{1}{2},0}) + (1 - \cos\theta_\ell)^2 H^2_{\frac{1}{2},1} + (1 + \cos\theta_\ell)^2 H^2_{-\frac{1}{2},-1}, \quad (48)$$

$$A_2 = 2\cos^2\theta_\ell (H^2_{\frac{1}{2},0} + H^2_{-\frac{1}{2},0}) + 2(H^2_{\frac{1}{2},t} + H^2_{-\frac{1}{2},t}) + \sin^2\theta_\ell (H^2_{\frac{1}{2},1} + H^2_{-\frac{1}{2},1} + H^2_{-\frac{1}{2},-1}) + 4\cos\theta_\ell (H_{\frac{1}{2},t} H_{\frac{1}{2},0} + H_{-\frac{1}{2},t} H_{-\frac{1}{2},0}). \quad (49)$$

Integration of Eq. (47) over $\cos\theta_\ell$ yields the q^2-dependent differential decay width:

$$\frac{d\Gamma(\Lambda_b \to \Lambda_c \ell^- \bar{\nu}_\ell)}{dq^2} = \int_{-1}^{1} \frac{d\Gamma(\Lambda_b \to \Lambda_c \ell^- \bar{\nu}_\ell)}{dq^2 d\cos\theta_\ell} d\cos\theta_\ell. \quad (50)$$

Since the masses of the electron and muon are negligible compared to those of the initial and final baryons, the SM predictions for the e and μ channels are nearly identical. Therefore, only the results for the μ and τ modes are discussed in the following.

To probe potential effects beyond the SM, it is essential to evaluate LFU, which is defined as Eq. (2). Our predictions for the branching fractions and LFU parameters

TABLE III. Comparison of theoretical predictions for the $\Lambda_b \to \Lambda_c$ semileptonic decay branching ratios and the LFU ratio.

Model	$\mathcal{B}(\Lambda_b \to \Lambda_c \mu \bar{\nu}_\mu)$	$\mathcal{B}(\Lambda_b \to \Lambda_c \tau \bar{\nu}_\tau)$	$\mathcal{R}_{\Lambda_c}$
This work	$(5.8^{+1.5}_{-2.0}) \times 10^{-2}$	$(1.7^{+0.4}_{-0.5}) \times 10^{-2}$	$0.29^{+0.12}_{-0.11}$
RQM [46]	6.48×10^{-2}	2.03×10^{-2}	0.313
CCQM [45]	6.9×10^{-2}	2.0×10^{-2}	0.29
QCDSR [43]	5.57×10^{-2}	1.54×10^{-2}	0.28
LQCD [6]	...	...	0.3318
HQET@NLP [7]	...	...	0.324 ± 0.004

are presented in Table III, along with results from other theoretical approaches for comparison. Owing to the heavier mass of the τ lepton, the corresponding decay channel is subject to kinematic suppression, leading to an expected LFU ratio R_{Λ_c} smaller than 1. From the table, it is found that for $\mathcal{R}_{\Lambda_c}$ our predictions are lower than the estimations of Refs. [6,46], but slightly higher than the value reported in Ref. [43]. The LHCb Collaboration has recently reported a measurement of the LFU ratio in the $\Lambda_b \to \Lambda_c \ell^- \bar{\nu}_\ell$ decay channel, obtaining $\mathcal{R}_{\Lambda c} = 0.242 \pm 0.026(\text{stat}) \pm 0.040(\text{syst}) \pm 0.059(\text{ext})$ [5], where the uncertainties correspond to statistical, systematic, and external branching fraction contributions, respectively. It is found that our result is slightly larger than the experimental data, corresponding to a tension of approximately 0.35σ. And we also note that this experimental result exhibits a 1.3σ tension with the SM prediction of $\mathcal{R}_{\Lambda_c} = 0.324 \pm 0.004$ [7], which incorporates both lattice QCD calculations and measured spectral information. This observed discrepancy may suggest a potential violation of LFU in semileptonic $\Lambda_b \to \Lambda_c \ell^- \bar{\nu}_\ell$ decays. Our theoretical predictions provide complementary insights into the study of LFU in the $b \to c \ell \bar{\nu}_\ell$ transitions and may serve as a useful reference for future experimental investigations.

It is worth emphasizing that the predicted branching fractions are subject to sizable theoretical uncertainties. These mainly arise from the modeling of hadronic form factors, uncertainties in the parameters of the LCDAs, and the omission of higher-order QCD and power corrections. Reducing these uncertainties—through improved nonperturbative QCD inputs, refined nonperturbative parameter extraction, and the inclusion of radiative and subleading contributions—will be essential for enhancing the precision and reliability of theoretical predictions in future studies.

In particular, the forward-backward asymmetry (A_{FB}) of the leptonic sector is of significant interest, as it exhibits reduced sensitivity to hadronic form factor uncertainties. It is defined as follows:

$$A_{FB}^{\ell}(q^2) = \frac{\int_0^1 \frac{d\Gamma}{dq^2 d\cos\theta_\ell} d\cos\theta_\ell - \int_{-1}^0 \frac{d\Gamma}{dq^2 d\cos\theta_\ell} d\cos\theta_\ell}{\int_0^1 \frac{d\Gamma}{dq^2 d\cos\theta_\ell} d\cos\theta_\ell + \int_{-1}^0 \frac{d\Gamma}{dq^2 d\cos\theta_\ell} d\cos\theta_\ell}. \tag{51}$$

In addition, other observables, such as the final state hadron polarization (P_B) and lepton polarization (P_ℓ), are defined as

$$P_\ell(q^2) = \frac{d\Gamma^{\lambda_\ell=1/2}/dq^2 - d\Gamma^{\lambda_\ell=-1/2}/dq^2}{d\Gamma^{\lambda_\ell=1/2}/dq^2 + d\Gamma^{\lambda_\ell=-1/2}/dq^2}, \tag{52}$$

$$P_B(q^2) = \frac{d\Gamma^{\lambda_{\Lambda_c}=1/2}/dq^2 - d\Gamma^{\lambda_{\Lambda_c}=-1/2}/dq^2}{d\Gamma^{\lambda_{\Lambda_c}=1/2}/dq^2 + d\Gamma^{\lambda_{\Lambda_c}=-1/2}/dq^2}, \tag{53}$$

and the differential widths with definite polarization of the final state can be written as

$$\frac{d\Gamma^{\lambda_{\Lambda_c}=1/2}}{dq^2} = \frac{4m_\ell^2}{3q^2}(H_{1/2,1}^2 + H_{1/2,0}^2 + 3H_{1/2,t}^2) + \frac{8}{3}(H_{1/2,0}^2 + H_{1/2,1}^2), \tag{54}$$

$$\frac{d\Gamma^{\lambda_{\Lambda_c}=-1/2}}{dq^2} = \frac{4m_\ell^2}{3q^2}(H_{-1/2,-1}^2 + H_{-1/2,0}^2 + 3H_{-1/2,t}^2) + \frac{8}{3}(H_{-1/2,0}^2 + H_{-1/2,-1}^2), \tag{55}$$

$$\frac{d\Gamma^{\lambda_\ell=1/2}}{dq^2} = \frac{m_\ell^2}{q^2}\left[\frac{4}{3}(H_{1/2,1}^2 + H_{1/2,0}^2 + H_{-1/2,-1}^2 + H_{-1/2,0}^2) + 4(H_{1/2,t}^2 + H_{-1/2,t}^2)\right], \tag{56}$$

$$\frac{d\Gamma^{\lambda_\ell=-1/2}}{dq^2} = \frac{8}{3}(H_{1/2,1}^2 + H_{1/2,0}^2 + H_{-1/2,-1}^2 + H_{-1/2,0}^2). \tag{57}$$

We also find that the differential angular distribution contains a large number of $\cos\theta_\ell$ terms. In order to better describe $\cos\theta_\ell$, the convexity parameter C_F is defined as the second derivative of the normalized angular distribution,

$$C_F^{\ell}(q^2) = \frac{1}{d\Gamma/dq^2}\frac{d^2}{d\cos^2\theta}\left(\frac{d^2\Gamma}{dq^2 d\cos\theta}\right). \tag{58}$$

TABLE IV. Comparison of theoretical predictions for the Λ_b semileptonic decay parameters with available theoretical approaches.

Model	ℓ	$\langle\Gamma\rangle$	$\langle A_{FB}\rangle$	$\langle P_B\rangle$	$\langle P_\ell\rangle$	$\langle C_F\rangle$
This work	e	26	$0.193^{+0.006}_{-0.001}$	$-0.928^{+0.001}_{-0.014}$	-1.0	$-0.751^{+0.002}_{-0.007}$
	μ	26	$0.182^{+0.009}_{-0.003}$	$-0.930^{+0.001}_{-0.011}$	-1.0	$-0.727^{+0.002}_{-0.007}$
	τ	7.7	$-0.076^{+0.002}_{-0.001}$	$-0.630^{+0.012}_{-0.002}$	$-0.173^{+0.007}_{-0.001}$	$-0.088^{+0.001}_{-0.001}$
RQM [46]	e	29.4	0.195	−0.80	⋯	−0.57
	μ	29.0	0.189	−0.80	⋯	−0.55
	τ	9.1	−0.021	−0.71	⋯	−0.09
CCQM [43]	e	32.0	0.36	−0.82	−1.00	−0.63
	μ	⋯	⋯	⋯	⋯	⋯
	τ	9.40	−0.077	−0.72	−0.32	−0.10
LFQM [39]	e	⋯	0.18	−0.81	−1.00	⋯
	μ	⋯	0.17	−0.81	−0.98	⋯
	τ	⋯	−0.08	−0.77	−0.24	⋯

In fact, it helps to disentangle the contributions from different helicity amplitudes. Since C_F can be extracted from the shape of the angular distribution, it is a robust observable for comparing experimental data with theoretical predictions. Deviations from SM expectations in C_F^ℓ may indicate new physics in the semileptonic decay processes.

In Table IV, we present our predictions for the averaged values of several key observables: the total decay width $\langle\Gamma\rangle$ (in units of 10^{-15} GeV), the forward-backward asymmetry of the charged lepton $\langle A_{FB}\rangle$, the polarization of the final-state baryon $\langle P_B\rangle$, the polarization of the charged lepton $\langle P_\ell\rangle$, and the lepton-side convexity parameter $\langle C_F^\ell\rangle$. These observables exhibit reduced sensitivity to model-dependent uncertainties, as many theoretical errors cancel in the ratios of helicity amplitudes. Significant variations are observed when transitioning from the light lepton (e/μ) to the τ channel, primarily due to the sizable mass of the τ lepton. Notably, the forward-backward asymmetry $\langle A_{FB}\rangle$ undergoes a sign reversal in the τ mode, reflecting the pronounced influence of helicity suppression effects. We further compare our results for the integrated observables with those obtained from other theoretical frameworks [39,43,46], as also summarized in Table IV. A good level of consistency is found among all theoretical predictions, which provides a promising basis for future experimental validation.

Using the analytical expressions of the observables derived in the previous sections, we plot their dependence on the momentum transfer squared q^2, as illustrated in the figure below. Figure 3 shows the q^2 dependence of the differential decay widths for the processes $\Lambda_b \to \Lambda_c \ell^- \bar{\nu}_\ell$, with $\ell = \mu, \tau$. According to Eq. (50), in the large-recoil region (i.e., $q^2 \to m_\ell^2$), the differential width displays a steplike behavior. Conversely, in the zero-recoil limit, the differential width vanishes.

Figure 4 shows the q^2 dependence of the lepton-side forward-backward asymmetry $A_{FB}^\ell(q^2)$, as defined in Eq. (51). At zero recoil, A_{FB}^ℓ vanishes for both the μ and τ channels due to the helicity relation $H^2_{1/2,1} = H^2_{-1/2,-1}$. In the large-recoil limit, $A_{FB}^\mu(q^2)$ also tends to zero, reflecting the dominance of longitudinal contributions to the decay rate. Notably, the behavior of $A_{FB}(q^2)$ differs significantly between the two lepton flavors: while $A_{FB}^\mu(q^2)$ almost remains positive across the entire q^2 spectrum, $A_{FB}^\tau(q^2)$ becomes negative shortly after zero recoil (i.e., $q^2 \to q^2_{\rm max}$) and crosses zero at $q^2 \approx 8.5$ GeV^2.

In Fig. 5, we present the q^2 dependence of the lepton polarization asymmetry $P_\ell(q^2)$ as defined in Eq. (52). For the μ-mode decays, the blue solid curve corresponds to the chiral limit ($m_\mu \to 0$) where the lepton becomes purely left handed. Figure 6 displays the Λ_c baryon polarization parameter derived from Eq. (53). For both modes, the

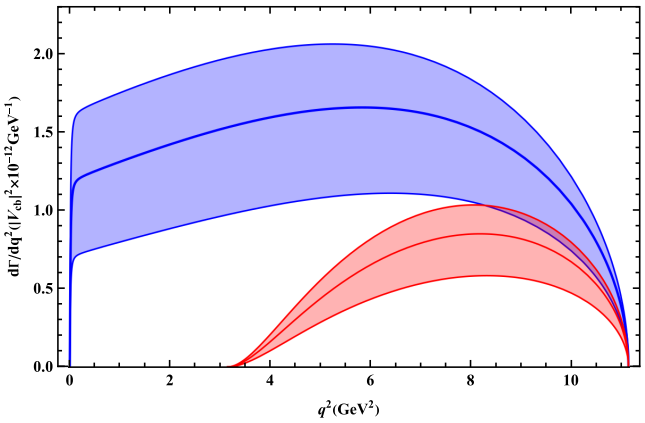


FIG. 3. The q^2 dependence of the differential widths for the $\Lambda_b \to \Lambda_c \ell \bar{\nu}_\ell$ decays with $\ell = \mu, \tau$.

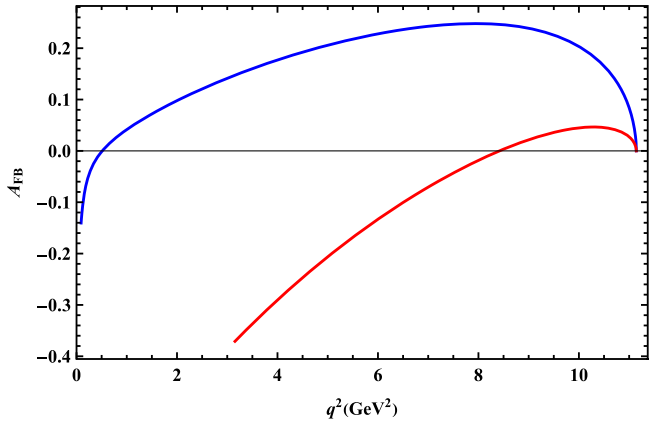


FIG. 4. The q^2 dependence of the lepton-side forward-backward asymmetry $A_{FB}^{\ell}(q^2)$ for the μ^-(blue) and τ^-(red) modes.

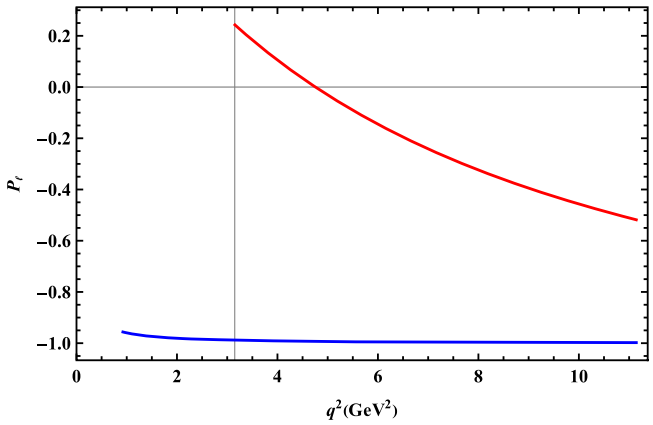


FIG. 5. The q^2 dependence of the lepton polarization P_ℓ for the μ^-(blue) and τ^-(red) modes.

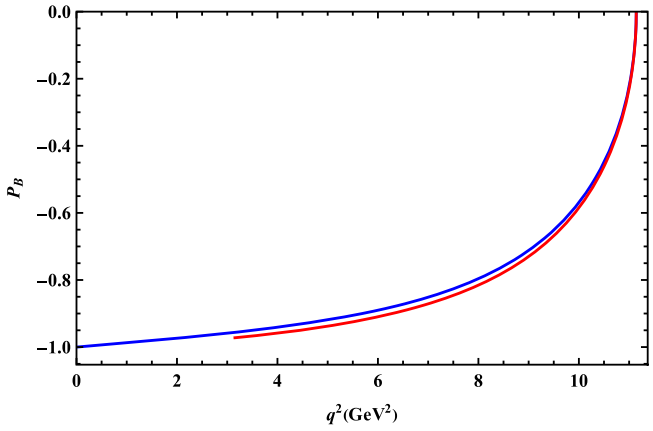


FIG. 6. The q^2 dependence of the polarization $P_B(q^2)$ of the daughter baryon Λ_c for the μ^-(blue) and τ^-(red) modes.

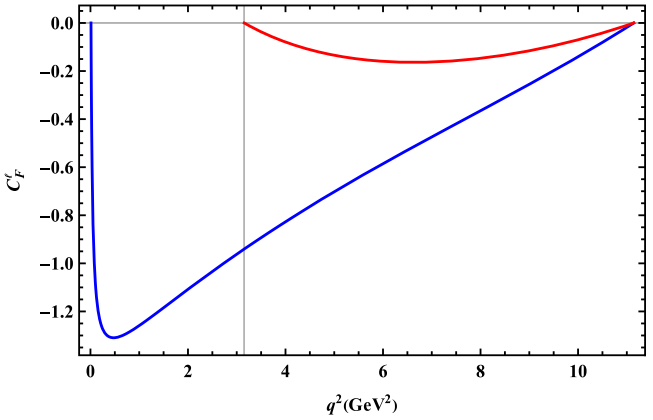


FIG. 7. The q^2 dependence of the convexity parameter $C_F^{\ell}(q^2)$ for the μ^-(blue) and τ^-(red) modes.

hadronic polarization vanishes at zero recoil as a consequence of the helicity amplitude relations $H_{1/2,1}^2 - H_{-1/2,-1}^2 = H_{1/2,0}^2 - H_{-1/2,0}^2 = H_{1/2,t}^2 - H_{-1/2,t}^2 = 0$ at zero recoil.

In Fig. 7, we show the q^2 dependence of the convexity parameter C_F, as defined in Eq. (58). At zero recoil, C_F^{ℓ} vanishes for both decay modes, which follows from the relation $H_{1/2,1}^2 + H_{-1/2,-1}^2 = 2(H_{1/2,0}^2 + H_{-1/2,0}^2)$. In the τ channel, C_F^{τ} also approaches zero near the kinematic threshold $q^2 = m_\tau^2$, where the ratio $m_\ell^2/q^2 \to 1$, in accordance with Eqs. (58) and (47). Over the full q^2 range accessible in the τ mode, C_F^{τ} remains small, indicating that the $\cos\theta_\ell$ distribution is nearly linear. In contrast, for the μ mode, C_F^{μ} can become significantly negative, corresponding to a strongly parabolic angular distribution characterized by a downward-opening curvature.

VI. SUMMARY

In this work, we calculate the transition form factors for the decay $\Lambda_b \to \Lambda_c$ using the pQCD approach and investigate the semileptonic decay $\Lambda_b \to \Lambda_c \ell^- \bar{\nu}_\ell$ within the SM. Six independent form factors are evaluated in the low-q^2 region and then extrapolated to the entire physical kinematic range by parametrizing their q^2 dependence using the z expansion, incorporating the latest lattice QCD results in the high-q^2 region. We also analyze the q^2 behavior of these form factors and find that their magnitudes generally increase with q^2, as expected for weak decays. Among them, the dominant contributions arise from the vector and axial-vector form factors $f_1(q^2)$ and $g_1(q^2)$, which exhibit very similar q^2 dependence. The remaining form factors, $f_{2,3}(q^2)$ and $g_{2,3}(q^2)$, are found to be negligibly small across the entire q^2 range, consistent with expectations from HQET. Our results at both the maximum and

minimum recoil points are compared with previous theoretical predictions obtained from various frameworks, including constituent quark models, QCD sum rules, and HQET, showing reasonable agreement.

Utilizing the calculated form factors and helicity formalism, we further investigate several experimentally relevant observables, including branching fractions, forward-backward asymmetries, the lepton-side convexity parameter, and final-state polarizations. Both of the differential and integrated observables across all lepton channels are calculated, which could be tested with future experiments. It is found that the shape of the differential distributions of these quantities for the τ mode is different from those for the μ mode due to the large τ-lepton mass effect. These predictions may confirm the SM or give complementary information regarding possible new physics in heavy baryon decays. In addition, we predict the lepton flavor universality (LFU) violating ratio $\mathcal{R}_{\Lambda_c} = 0.29^{+0.12}_{-0.11}$ that shows good consistency with existing available predictions. However, our result is slightly larger than the latest experimental data [5], $\mathcal{R}_{\Lambda_c} = 0.242 \pm 0.026(\text{stat}) \pm 0.040(\text{syst}) \pm 0.059(\text{ext})$, corresponding to a tension of approximately 0.35σ. Although not statistically significant, this mild deviation may hint at a potential violation of LFU in semileptonic $\Lambda_b \to \Lambda_c \ell^- \bar{\nu}_\ell$ decays.

We acknowledge that there are considerable theoretical uncertainties in our calculations. In particular, the limited precision of the LCDAs of heavy baryons introduces sizable model dependence in the form factor calculations. Future improvements on this front are essential, including lattice QCD determinations of higher-order LCDA moments and more refined QCD sum rule analyses. Additionally, subleading contributions in the perturbative expansion, such as next-to-leading-order corrections in α_s, and higher-twist effects beyond the leading-power factorization, must be systematically incorporated to reduce theoretical uncertainties. The inclusion of $1/m_Q$ power corrections within HQET and pQCD frameworks may further enhance the fidelity of the predictions. Such efforts will not only improve the accuracy of $\Lambda_b \to \Lambda_c$ form factors but also increase the reliability of Standard Model benchmarks against which potential new physics effects can be probed.

ACKNOWLEDGMENTS

This work is supported in part by the National Science Foundation of China under the Grants No. 12375089 and No. 12435004, and the Natural Science Foundation of Shandong Province under the Grants No. ZR2022ZD26 and No. ZR2022MA035.

DATA AVAILABILITY

The data that support the findings of this article are not publicly available upon publication because it is not technically feasible and/or the cost of preparing, depositing, and hosting the data would be prohibitive within the terms of this research project. The data are available from the authors upon reasonable request.

APPENDIX: THE DETAILED PROCESS OF CALCULATING FORM FACTORS USING FACTORIZABLE DIAGRAMS

The virtualities of two internal gluons and two quarks for each diagram T_i in Fig. 1 are collected in Table V. The inner functions B_{T_i} from the denominators of the internal propagators in diagrams T_i are presented in Table VI, where the functions h_l are defined as

$$h_1 = \int_0^1 \frac{dz_1 dz_2}{z_1(1-z_1)} \frac{\sqrt{X_1}}{\sqrt{|Y_1|}} \pi^2 K_1\left(\sqrt{X_1 Y_1}\right), \tag{A1}$$

$$h_2 = \int_0^1 dz \frac{|\mathbf{b}_2 + \mathbf{b}_2'|}{\sqrt{|X_2|}} \left\{ \pi K_1\left(\sqrt{X_2}|\mathbf{b}_2 + \mathbf{b}_2'|\right)\theta(X_2) + \frac{\pi^2}{2}\left[N_1\left(\sqrt{|X_2|}|\mathbf{b}_2 + \mathbf{b}_2'|\right) - iJ\left(\sqrt{|X_2|}|\mathbf{b}_2 + \mathbf{b}_2'|\right)\right]\theta(-X_2)\right\}, \tag{A2}$$

$$h_3 = 2\pi K_0\left(\sqrt{t_D^{T_6}}|\mathbf{b}_3 + \mathbf{b}_3'|\right)\theta(t_D^{T_6}) + \pi^2\left[-N_0\left(\sqrt{|t_D^{T_6}|}|\mathbf{b}_3 + \mathbf{b}_3'|\right) + iJ_0\left(\sqrt{|t_D^{T_6}|}|\mathbf{b}_3 + \mathbf{b}_3'|\right)\right]\theta(-t_D^{T_6}). \tag{A3}$$

$$h_4 = 2\pi K_0\left(\sqrt{t_D^{T_7}}|\mathbf{b}_3 + \mathbf{b}_3'|\right)\theta(t_D^{T_7}) + \pi^2\left[-N_0\left(\sqrt{|t_D^{T_7}|}|\mathbf{b}_3 + \mathbf{b}_3'|\right) + iJ_0\left(\sqrt{|t_D^{T_7}|}|\mathbf{b}_3 + \mathbf{b}_3'|\right)\right]\theta(-t_D^{T_7}). \tag{A4}$$

$$h_5 = \int_0^1 \frac{dz_1 dz_2}{z_1(1-z_1)} \frac{\sqrt{X_3}}{\sqrt{|Y_3|}} \left\{ \pi^2 K_1\left(\sqrt{X_3 Y_3}\right)\theta(Y_3) + \frac{\pi^3}{2}\left[N_1\left(\sqrt{X_3|Y_3|}\right) - iJ_1\left(\sqrt{X_3|Y_3|}\right)\right]\theta(-Y_3)\right\}, \tag{A5}$$

with

$$X_1 = |(1-z_1)\mathbf{b}_2' + z_1\mathbf{b}_2|^2 + \frac{z_1(1-z_1)}{z_2}|\mathbf{b}_2 + \mathbf{b}_2'|^2, \qquad Y_1 = t_B^{T_3}(1-z_2) + \frac{z_2}{z_1(1-z_1)}\{t_C^{T_3}(1-z_1) + t_D^{T_3} z_1\}. \tag{A6}$$

TABLE V. The virtualities of the internal gluon $t_{A,B}^{T_i}$ and quark $t_{C,D}^{T_i}$ for diagram $T_1, T_2, T_3, T_5, T_6, T_7, T_9$ in Fig. 1.

T_i	$t_A^{T_i}$	$t_B^{T_i}$	$t_C^{T_i}$	$t_D^{T_i}$
T_1	$m_{\Lambda_b}^2 x_3 x_3'$	$m_{\Lambda_b}^2(1-x_1)(1-x_1')$	$m_{\Lambda_b}^2(1-x_1)x_3'$	$m_{\Lambda_b}^2(1-x_1')$
T_2	$m_{\Lambda_b}^2 x_3 x_3'$	$m_{\Lambda_b}^2(1-x_1)(1-x_1')$	$m_{\Lambda_b}^2(1-x_1)x_3'$	$m_{\Lambda_b}^2(1-x_1')$
T_3	$m_{\Lambda_b}^2 x_3 x_3'$	$m_{\Lambda_b}^2 x_2 x_2'$	$m_{\Lambda_b}^2(x_2+x_3'-x_2x_3')$	$m_{\Lambda_b}^2(1-x_1')$
T_5	$m_{\Lambda_b}^2 x_3 x_3'$	$m_{\Lambda_b}^2 x_2 x_2'$	$m_{\Lambda_b}^2(x_2'+x_3-x_2'x_3)$	$m_{\Lambda_b}^2[r_c^2+(1-x_2')(x_3-r^2)]$
T_6	$m_{\Lambda_b}^2 x_3 x_3'$	$m_{\Lambda_b}^2(1-x_1)(1-x_1')$	$m_{\Lambda_b}^2(1-x_1)x_3'$	$m_{\Lambda_b}^2(1+r_c^2-r^2-x_1)$
T_7	$m_{\Lambda_b}^2 x_3 x_3'$	$m_{\Lambda_b}^2(1-x_1)(1-x_1')$	$m_{\Lambda_b}^2(1-x_1')x_3$	$m_{\Lambda_b}^2(1+r_c^2-r^2-x_1)$
T_9	$m_{\Lambda_b}^2 x_3 x_3'$	$m_{\Lambda_b}^2 x_2 x_2'$	$m_{\Lambda_b}^2(1+r_c^2-r^2-x_1)$	$m_{\Lambda_b}^2[r_c^2+x_2+r^2(x_3'-1)-x_2x_3']$

TABLE VI. The expressions of B_{T_i} for diagrams $T_1, T_2, T_3, T_5, T_6, T_7, T_9$ in Fig. 1.

T_i	B_{T_i}
T_1	$\frac{1}{(2\pi)^4}K_0(\sqrt{t_A}\lvert\mathbf{b}_2-\mathbf{b}_3\rvert)K_0(\sqrt{t_B}\lvert\mathbf{b}_3+\mathbf{b}_3'-\mathbf{b}_2'\rvert)K_0(\sqrt{t_C}\lvert\mathbf{b}_2-\mathbf{b}_3+\mathbf{b}_2'-\mathbf{b}_3'\rvert)K_0(\sqrt{t_D}\lvert\mathbf{b}_3+\mathbf{b}_3'\rvert)$
T_2	$\frac{1}{(2\pi)^4}K_0(\sqrt{t_A}\lvert\mathbf{b}_2-\mathbf{b}_3\rvert)K_0(\sqrt{t_B}\lvert\mathbf{b}_2\rvert)K_0(\sqrt{t_C}\lvert\mathbf{b}_2'-\mathbf{b}_3'+\mathbf{b}_2-\mathbf{b}_3\rvert)K_0(\sqrt{t_D}\lvert\mathbf{b}_3+\mathbf{b}_3'\rvert)$
T_3	$\frac{1}{(2\pi)^5}K_0(\sqrt{t_A}\lvert\mathbf{b}_3\rvert)h_1$
T_5	$\frac{1}{(2\pi)^4}K_0(\sqrt{t_A}\lvert\mathbf{b}_3'\rvert)K_0(\sqrt{t_B}\lvert\mathbf{b}_2\rvert)h_2$
T_6	$\frac{1}{(2\pi)^5}K_0(\sqrt{t_A}\lvert\mathbf{b}_2-\mathbf{b}_3\rvert)K_0(\sqrt{t_B}\lvert\mathbf{b}_2'\rvert)K_0(\sqrt{t_C}\lvert\mathbf{b}_2-\mathbf{b}_3+\mathbf{b}_2'-\mathbf{b}_3'\rvert)h_3$
T_7	$\frac{1}{(2\pi)^5}K_0(\sqrt{t_A}\lvert\mathbf{b}_2'-\mathbf{b}_3'\rvert)K_0(\sqrt{t_B}\lvert\mathbf{b}_2-\mathbf{b}_3-\mathbf{b}_3'\rvert)K_0(\sqrt{t_C}\lvert\mathbf{b}_2-\mathbf{b}_3+\mathbf{b}_2'-\mathbf{b}_3'\rvert)h_4$
T_9	$\frac{1}{(2\pi)^5}K_0(\sqrt{t_B}\lvert\mathbf{b}_2'\rvert)h_5$

$$X_2 = t_C^{T_5} z + t_D^{T_5}(1-z). \tag{A7}$$

$$X_3 = |-\mathbf{b}_2'-\mathbf{b}_2+\mathbf{b}_3'+z_1(\mathbf{b}_2+\mathbf{b}_2')|^2+\frac{z_1(1-z_1)}{z_2}|\mathbf{b}_2+\mathbf{b}_2'|^2,$$
$$Y_3 = t_A^{T_9}(1-z_2)+\frac{z_2}{z_1(1-z_1)}[t_C^{T_9}(1-z_1)+t_D^{T_9}z_1], \tag{A8}$$

with the Bessel functions $K_{0,1}$, $N_{0,1}$, and J_1 and $\theta(x)$ is a θ function. Below we provide the Fourier integration formula and various Bessel functions used in calculating the form factor. Among them, the Bessel function K_n has such a relationship with the first type of Bessel function J_n and the second type of Bessel function N_n:

$$K_n(-iz) = \frac{i\pi}{2}e^{(in\pi)/2}[J_n(z)+iN_n(z)] \tag{A9}$$

$$\int d^2k_T \frac{e^{i\mathbf{k}_T\cdot\mathbf{b}}}{k_T^2+A} = 2\pi K_0(\sqrt{A|\mathbf{b}|})\theta(A)+\pi^2[-N_0(\sqrt{|A|}|\mathbf{b}|)+iJ_0(\sqrt{|A|}|\mathbf{b}|)]\theta(-A), \tag{A10}$$

$$\int d^2k_T \frac{e^{i\mathbf{k}_T\cdot\mathbf{b}}}{(k_T^2+A)(k_T^2+B)} = \int_0^1 dz \frac{|\mathbf{b}|}{\sqrt{|\mathbf{Z}_1|}}\left\{\pi K_1(\sqrt{Z_1}|\mathbf{b}|)\theta(Z_1)+\frac{\pi^2}{2}[N_1(\sqrt{|Z_1|}|\mathbf{b}|)-iJ_1(\sqrt{|Z_1|}|\mathbf{b}|)]\theta(-Z_1)\right\}, \tag{A11}$$

$$\int d^2k_{1T}d^2k_{2T}\frac{e^{i\mathbf{k}_{1T}\cdot\mathbf{b}_1+\mathbf{k}_{2T}\cdot\mathbf{b}_2}}{(k_{1T}^2+A)(k_{2T}^2+B)[(k_{1T}+k_{2T})^2+C]} = \int_0^1 \frac{dz_1dz_2}{z_1(1-z_1)}\frac{\sqrt{Y}}{\sqrt{|Z_2|}}\{\pi^2K_1(\sqrt{YZ_2})\theta(Z_2)$$
$$+\frac{\pi^3}{2}[N_1(\sqrt{Y|Z_2|})-iJ_1(\sqrt{Y|Z_2|})]\theta(-Z_2)\}, \tag{A12}$$

and the parameters Z_1, Z_2, and Y are given by

$$Z_1 = zA + (1-z)B, \tag{A13}$$

$$Z_2 = (1-z_2)A + \frac{z_2}{z_1(1-z_1)}[(1-z_1)B + z_1 C], \tag{A14}$$

$$Y = (\mathbf{b}_1 - z_1\mathbf{b}_2)^2 + \frac{z_1(1-z_1)}{z_2}\mathbf{b}_2^2. \tag{A15}$$

The formulas of the hard scatter function $H_k(x_i, x_i')$ from the Feynman diagrams are as shown below:

$$H_{f_1}^{T_1} = H_{g_1}^{T_1} = 8m_{\Lambda_b}^2\{x_3'(2r-1) - (x_1-1)x_1'(r-2)r\}, \tag{A16}$$

$$H_{f_2}^{T_1} = H_{f_3}^{T_1} = \frac{8m_{\Lambda_b}^4}{(r^2-1)}\{(x_1'-1)(1-x_1)(r-2)r\}, \tag{A17}$$

$$H_{g_2}^{T_1} = H_{g_3}^{T_1} = \frac{8m_{\Lambda_b}^4}{(r^2-1)}\{(x_1'-1)(x_1-1)(r-2)r\}, \tag{A18}$$

$$H_{f_1}^{T_2} = H_{g_1}^{T_2} = -8m_{\Lambda_b}^4\{x_1'(r^2 - 2(x_3+1)r + x_3) - (r-2)r\}, \tag{A19}$$

$$H_{f_2}^{T_2} = H_{f_3}^{T_2} = \frac{8m_{\Lambda_b}^4}{(r^2-1)}\{(x_1'-1)x_3(2r-1)\}, \tag{A20}$$

$$H_{g_2}^{T_2} = H_{g_3}^{T_2} = -\frac{8m_{\Lambda_b}^4}{(r^2-1)}\{(x_1'-1)x_3(2r-1)\}, \tag{A21}$$

$$H_{f_1}^{T_3} = H_{g_1}^{T_3} = 4m_{\Lambda_b}^4\{r(2x_1'r + r - 2)x_3' + x_3' + x_2(x_1'(r-1)^2 + 2) - 2(r+1)(x_1'r+1)\}, \tag{A22}$$

$$H_{f_2}^{T_3} = H_{f_3}^{T_3} = \frac{4m_{\Lambda_b}^4}{r^2-1}(x_1'-1)\{r^2(x_2 + 2x_3' - 2) - 2(x_2+1)r + x_2\}, \tag{A23}$$

$$H_{g_2}^{T_3} = H_{g_3}^{T_3} = -\frac{4m_{\Lambda_b}^4}{r^2-1}(x_1'-1)\{r^2(x_2 + 2x_3' - 2) - 2(x_2+1)r + x_2\}, \tag{A24}$$

$$H_{f_1}^{T_5} = -4m_{\Lambda_b}^4\{(x_2'-1)x_2'r^3 + r^2(2(r_c+1) - x_2')(r_c+2)) + (x_2'-1)(x_2' - 2(r_c+1))r + x_2'r_c\}, \tag{A25}$$

$$H_{f_2}^{T_5} = \frac{4m_{\Lambda_b}^4}{(r^2-1)^2}\{(r-1)r(r^2+1)x_2'^2 - r_c x_2' + 2r(-r^2 + x_3 + 1)(r - r_c) + r(-3r + (r-1)(r(r-r_c) - 2x_3) + 3r_c + 1)x_2'\}, \tag{A26}$$

$$H_{f_3}^{T_5} = \frac{-4m_{\Lambda_b}^4}{(1-r^2)^2}(r-1)\{-2(r^2+1)x_3^2 + 2r((r+1)(r^2 - r_c r + 2r_c + 2) - x_2'(r+1)^2)x_3 + x_2'^2 r(r^2+1)^2 + 2(r-1)r(r+1)^2(r_c - r) + x_2'(r+1)(r_c + r(-3r_c + r(r(r(r-r_c-5) + r_c - 1) - 1) - 1))\}, \tag{A27}$$

$$H_{g_1}^{T_5} = 4m_{\Lambda_b}^4\{(x_2'-1)r((r-4)rx_2' + x_2' + 2(r+1)) + (r(3r-2)x_2' + x_2' - 2r(r+1))r_c\}, \tag{A28}$$

$$H_{g_2}^{T_5} = \frac{-4m_{\Lambda_b}^4}{(r^2-1)}\{r(r+1)((r-4)r+1)x_2'^2 + (r_c - r(-2x_3(r+1) + r_c + r(r(3r - 3r_c - 5) + r_c - 5) + 1))x_2' + 2r(r^2-1)(r - r_c) - 2x_3 r(r + r_c + 2)\}, \tag{A29}$$

$$H_{g_3}^{T_5} = \frac{4m_{\Lambda_b}^4}{(1-r^2)^2}(r+1)\{r((r-4)r+1)(r^2+1)x_2'^2 - (r-1)(3r^3 - r^2 + r - 1)(r - r_c)x_2' + 2x_3^2((r-4)r+1) + 2x_3 r(x_2'(r+1)^2 - (r-2)(r-1)(r-r_c)) + 2(r-1)^2 r(r+1)(r-r_c)\}. \tag{A30}$$

$$H_{f_1}^{T_6} = H_{g_1}^{T_6} = -8m_{\Lambda_b}^4 r\{x_1(r-2) + x_3' r_c - r(2x_3' r_c + 1) + 2\}, \tag{A31}$$

$$H_{f_2}^{T_6} = H_{g_2}^{T_6} = \frac{8m_{\Lambda_b}^4 r}{(r^2-1)^2}\{(x_1-1)(r-2)(r-r_c) + x_3'(2r-1)(r^2 - r_c r + x_1 - 1)\}, \tag{A32}$$

$$H_{f_3}^{T_6} = H_{g_3}^{T_6} = -\frac{8m_{\Lambda_b}^4 r}{(r^2-1)^2}\{(x_1-1)(r-2)(r-r_c) + x_3'(2r-1)(r^2 - r_c r + x_1 - 1)\}, \tag{A33}$$

$$H_{f_1}^{T_7} = H_{g_1}^{T_7} = -8m_{\Lambda_b}^4\{(x_1'-1)(r-2)r_c r^2 - 2x_3 r + x_3\}, \tag{A34}$$

$$H_{f_2}^{T_7} = H_{g_2}^{T_7} = -\frac{8m_{\Lambda_b}^4}{(r^2-1)}\{(x_1'-1)(r-2)(r^2 - r_c r + x_1 - 1)r^2 + x_3(2r-1)(r-r_c)\}, \tag{A35}$$

$$H_{f_3}^{T_7} = H_{g_3}^{T_7} = \frac{8m_{\Lambda_b}^4}{(r^2-1)}\{(x_1'-1)(r-2)(r^2 - r_c r + x_1 - 1)r^2 + x_3(2r-1)(r-r_c)\}, \tag{A36}$$

$$\begin{aligned} H_{f_1}^{T_9} = H_{g_1}^{T_9} = -4m_{\Lambda_b}^4\{&(-2x_3' + (r-2)r + 2)r^2 - ((x_3'-2)r^2 - 2(x_3'+1)r + x_3' + 2)r_c r + x_3(r + 2r_c - 2)r + 2r \\ &- ((r-4)r+1)r_c^2 + x_3 + x_1((r-1)^2 + 2rr_c) - 1\} \end{aligned} \tag{A37}$$

$$\begin{aligned} H_{f_2}^{T_9} = H_{g_2}^{T_9} = \frac{4m_{\Lambda_b}^4}{r^2-1}\{&(x_3'-2)r^5 - (x_3'(r_c+2) - 2r_c)r^4 + (-x_3 + x_1(x_3'-4) + 2x_3'(r_c-1) + 6)r^3 \\ &+ ((2x_1 + x_3 + x_3' - 4)r_c - 2(x_3 + (x_1-1)x_3'))r^2 + (-2x_1^2 + (-2x_3 + x_3' - 2r_c + 4)x_1 + 3x_3 - x_3' \\ &+ 2(x_3+1)r_c - 2)r - x_3 r_c\} \end{aligned} \tag{A38}$$

$$\begin{aligned} H_{f_3}^{T_9} = H_{g_3}^{T_9} = \frac{4m_{\Lambda_b}^4}{r^2-1}\{&-((x_3'-2)r^5) + (x_3'(r_c+2) - 2r_c)r^4 + (x_3 - x_1(x_3'-4) + 2x_3' - 2x_3' r_c - 6)r^3 \\ &+ (2(x_3 + (x_1-1)x_3') - (2x_1 + x_3 + x_3' - 4)r_c)r^2 \\ &+ (-3x_3 + 2x_1(x_1 + x_3 - 2) - x_1 x_3' + x_3' + 2(x_1 - x_3)r_c - 2r_c + 2)r + x_3 r_c\}. \end{aligned} \tag{A39}$$

[1] S. Banerjee *et al.* (Heavy Flavor Averaging Group (HFLAV)), Averages of b-hadron, c-hadron, and τ-lepton properties as of 2023, arXiv:2411.18639.

[2] F. U. Bernlochner, Z. Ligeti, M. Papucci, and D. J. Robinson, Combined analysis of semileptonic B decays to D and D^*: $R(D^{(*)})$, $|V_{cb}|$, and new physics, Phys. Rev. D **95**, 115008 (2017); **97**, 059902(E) (2018).

[3] B. Capdevila, A. Crivellin, and J. Matias, Review of semileptonic B anomalies, Eur. Phys. J. Special Topics **233**, 409 (2024).

[4] S. Bifani, S. Descotes-Genon, A. Romero Vidal, and M.-H. Schune, Review of lepton universality tests in B decays, J. Phys. G **46**, 023001 (2019).

[5] R. Aaij *et al.* (LHCb Collaboration), Observation of the decay $\Lambda_b^0 \to \Lambda_c^+ \tau^- \bar{\nu}_\tau$, Phys. Rev. Lett. **128**, 191803 (2022).

[6] W. Detmold, C. Lehner, and S. Meinel, $\Lambda_b \to p\ell^-\bar{\nu}_\ell$ and $\Lambda_b \to \Lambda_c \ell^- \bar{\nu}_\ell$ form factors from lattice QCD with relativistic heavy quarks, Phys. Rev. D **92**, 034503 (2015).

[7] F. U. Bernlochner, Z. Ligeti, D. J. Robinson, and W. L. Sutcliffe, Precise predictions for $\Lambda_b \to \Lambda_c$ semileptonic decays, Phys. Rev. D **99**, 055008 (2019).

[8] H.-H. Duan, Y.-L. Liu, and M.-Q. Huang, Light-cone sum rule analysis of semileptonic decays $\Lambda_b^0 \to \Lambda_c^+ \ell^- \bar{\nu}_\ell$, Eur. Phys. J. C **82**, 951 (2022).

[9] X.-L. Mu, Y. Li, Z.-T. Zou, and B. Zhu, Investigation of effects of new physics in $\Lambda_b \to \Lambda_c \tau \bar{\nu}_\tau$ decay, Phys. Rev. D **100**, 113004 (2019).

[10] M. Fedele, M. Blanke, A. Crivellin, S. Iguro, T. Kitahara, U. Nierste, and R. Watanabe, Impact of $\Lambda_b \to \Lambda_c \tau\nu$ measurement on new physics in $b \to c l \nu$ transitions, Phys. Rev. D **107**, 055005 (2023).

[11] S. Nandi, S. Sahoo, and R. Sain, An imperative study of the angular observables in $\Lambda_b \to \Lambda_c^+ (\to \Lambda\pi^+)\ell^-\bar{\nu}_\ell$ decay and probing the footprint of new physics, J. High Energy Phys. 11 (2024) 053.

[12] H.-n. Li, QCD aspects of exclusive B meson decays, Prog. Part. Nucl. Phys. **51**, 85 (2003).

[13] Y.-Y. Keum, H.-n. Li, and A. I. Sanda, Fat penguins and imaginary penguins in perturbative QCD, Phys. Lett. B **504**, 6 (2001).

[14] C.-D. Lu, K. Ukai, and M.-Z. Yang, Branching ratio and *CP* violation of $B-\to \pi\pi$ decays in perturbative QCD approach, Phys. Rev. D **63**, 074009 (2001).

[15] H.-H. Shih, S.-C. Lee, and H.-n. Li, The $\Lambda_b \to p\ell\bar{\nu}$ decay in perturbative QCD, Phys. Rev. D **59**, 094014 (1999).

[16] J.-J. Han, Y. Li, H.-n. Li, Y.-L. Shen, Z.-J. Xiao, and F.-S. Yu, $\Lambda_b \to p$ transition form factors in perturbative QCD, Eur. Phys. J. C **82**, 686 (2022).

[17] J.-J. Lei Yang, Q. C. Han, and F.-S. Yu, The $\Lambda_b \to \Lambda$ transition form factors in perturbative QCD approach, arXiv:2508.18069.

[18] H.-H. Shih, S.-C. Lee, and H.-n. Li, Applicability of perturbative QCD to $\Lambda_b \to \Lambda_c$ decays, Phys. Rev. D **61**, 114002 (2000).

[19] C.-D. Lu, Y.-M. Wang, H. Zou, A. Ali, and G. Kramer, Anatomy of the PQCD approach to the baryonic decays $\Lambda_b \to p\pi, pK$, Phys. Rev. D **80**, 034011 (2009).

[20] C.-H. Chou, H.-H. Shih, S.-C. Lee, and H.-n. Li, $\Lambda_b \to \Lambda J/\psi$ decay in perturbative QCD, Phys. Rev. D **65**, 074030 (2002).

[21] C.-Q. Zhang, J.-M. Li, M.-K. Jia, and Z. Rui, Nonleptonic two-body decays of $\Lambda_b \to \Lambda_c \pi$, $\Lambda_b \to \Lambda_c K$ in the perturbative QCD approach, Phys. Rev. D **105**, 073005 (2022).

[22] Z. Rui, Z.-T. Zou, Y. Li, and Y. Li, Semileptonic baryon decays $\Xi_b \to \Xi_c \ell^- \bar{\nu}_\ell$ in perturbative QCD, Phys. Rev. D **111**, 113006 (2025).

[23] H.-n. Li and G. F. Sterman, The perturbative pion form-factor with Sudakov suppression, Nucl. Phys. **B381**, 129 (1992).

[24] T. Kurimoto, H.-n. Li, and A. I. Sanda, Leading power contributions to $B \to \pi, \rho$ transition form-factors, Phys. Rev. D **65**, 014007 (2002).

[25] Y.-M. Wang, Y.-L. Shen, and C.-D. Lu, $\Lambda_b \to p, \Lambda$ transition form factors from QCD light-cone sum rules, Phys. Rev. D **80**, 074012 (2009).

[26] A. Khodjamirian, C. Klein, T. Mannel, and Y. M. Wang, Form factors and strong couplings of heavy baryons from QCD light-cone sum rules, J. High Energy Phys. 09 (2011) 106.

[27] Y.-M. Wang and Y.-L. Shen, Perturbative corrections to $\Lambda_b \to \Lambda$ form factors from QCD light-cone sum rules, J. High Energy Phys. 02 (2016) 179.

[28] Y. Miao, H. Deng, K.-S. Huang, J. Gao, and Y.-L. Shen, $\Lambda_b \to \Lambda_c$ form factors from QCD light-cone sum rules*, Chin. Phys. C **46**, 113107 (2022).

[29] J. Botts and G. F. Sterman, Hard Elastic Scattering in QCD: Leading Behavior, Nucl. Phys. **B325**, 62 (1989).

[30] B. Kundu, H.-n. Li, J. Samuelsson, and P. Jain, The perturbative proton form-factor reexamined, Eur. Phys. J. C **8**, 637 (1999).

[31] H.-n. Li and K. Ukai, Threshold resummation for nonleptonic B meson decays, Phys. Lett. B **555**, 197 (2003).

[32] T. Kurimoto, H.-n. Li, and A. I. Sanda, $B \to D^{(*)}$ form-factors in perturbative QCD, Phys. Rev. D **67**, 054028 (2003).

[33] W. Loinaz and R. Akhoury, Exclusive semileptonic decays of b baryons into protons, Phys. Rev. D **53**, 1416 (1996).

[34] F. Schlumpf, Relativistic constituent quark model for baryons, arXiv:hep-ph/9211255.

[35] X.-G. He, T. Li, X.-Q. Li, and Y.-M. Wang, Calculation of $\mathrm{BR}(\bar{B}^0 \to \Lambda_c^+ + \bar{p})$ in the PQCD approach, Phys. Rev. D **75**, 034011 (2007).

[36] P. Ball, V. M. Braun, and E. Gardi, Distribution amplitudes of the Λ_b baryon in QCD, Phys. Lett. B **665**, 197 (2008).

[37] G. Bell, T. Feldmann, Y.-M. Wang, and M. W. Y. Yip, Light-cone distribution amplitudes for heavy-quark hadrons, J. High Energy Phys. 11 (2013) 191.

[38] A. Ali, C. Hambrock, and A. Y. Parkhomenko, Light-cone wave functions of heavy baryons, Theor. Math. Phys. **170**, 2 (2012).

[39] Y.-S. Li, X. Liu, and F.-S. Yu, Revisiting semileptonic decays of $\Lambda_{b(c)}$ supported by baryon spectroscopy, Phys. Rev. D **104**, 013005 (2021).

[40] W. Detmold, C. J. D. Lin, S. Meinel, and M. Wingate, $\Lambda_b \to p l^- \bar{\nu}_\ell$ form factors from lattice QCD with static b quarks, Phys. Rev. D **88**, 014512 (2013).

[41] S. Meinel, $\Lambda_c \to \Lambda l^+ \nu_l$ form factors and decay rates from lattice QCD with physical quark masses, Phys. Rev. Lett. **118**, 082001 (2017).

[42] T. Gutsche, M. A. Ivanov, J. G. Körner, V. E. Lyubovitskij, and P. Santorelli, Heavy-to-light semileptonic decays of Λ_b and Λ_c baryons in the covariant confined quark model, Phys. Rev. D **90**, 114033 (2014); **94**, 059902(E) (2016).

[43] T. Gutsche, M. A. Ivanov, J. G. Körner, V. E. Lyubovitskij, P. Santorelli, and N. Habyl, Semileptonic decay $\Lambda_b \to \Lambda_c + \tau^- + \overline{\nu_\tau}$ in the covariant confined quark model, Phys. Rev. D **91**, 074001 (2015).

[44] Z.-X. Zhao, R.-H. Li, Y.-L. Shen, Y.-J. Shi, and Y.-S. Yang, The semi-leptonic form factors of $\Lambda_b \to \Lambda_c$ and $\Xi_b \to \Xi_c$ in QCD sum rules, Eur. Phys. J. C **80**, 1181 (2020).

[45] J. Zhu, Z.-T. Wei, and H.-W. Ke, Semileptonic and nonleptonic weak decays of Λ_b^0, Phys. Rev. D **99**, 054020 (2019).

[46] R. N. Faustov and V. O. Galkin, Semileptonic decays of Λ_b baryons in the relativistic quark model, Phys. Rev. D **94**, 073008 (2016).

[47] H.-W. Ke, X.-Q. Li, and Z.-T. Wei, Diquarks and $\Lambda_b \to \Lambda_c$ weak decays, Phys. Rev. D **77**, 014020 (2008).

[48] Z.-X. Zhao, Weak decays of heavy baryons in the light-front approach, Chin. Phys. C **42**, 093101 (2018).

[49] C.-K. Chua, Color-allowed bottom baryon to s-wave and p-wave charmed baryon nonleptonic decays, Phys. Rev. D **100**, 034025 (2019).

[50] H.-W. Ke, N. Hao, and X.-Q. Li, Revisiting $\Lambda_b \to \Lambda_c$ and $\Sigma_b \to \Sigma_c$ weak decays in the light-front quark model, Eur. Phys. J. C **79**, 540 (2019).

[51] K. Azizi, A. T. Olgun, and Z. Tavukoğlu, Effects of vector leptoquarks on $\Lambda_b \to \Lambda_c \ell \bar{\nu}_\ell$ decay, Chin. Phys. C **45**, 013113 (2021).

[52] K. Azizi and J. Y. Süngü, Semileptonic $\Lambda_b \to \Lambda_c \ell \bar{\nu}_\ell$ transition in full QCD, Phys. Rev. D **97**, 074007 (2018).

[53] S. Shivashankara, W. Wu, and A. Datta, $\Lambda_b \to \Lambda_c \tau \bar{\nu}_\tau$ Decay in the standard model and with new physics, Phys. Rev. D **91**, 115003 (2015); **109**, 119904(E) (2024).

[54] R. Dutta, $\Lambda_b \to (\Lambda_c, p)\tau\nu$ decays within standard model and beyond, Phys. Rev. D **93**, 054003 (2016).

[55] R. Zwicky, Endpoint symmetries of helicity amplitudes, Nucl. Phys. **B975**, 115673 (2022).
[56] G. Hiller and R. Zwicky, Endpoint relations for baryons, J. High Energy Phys. 11 (2021) 073.
[57] M. A. Ivanov, J. G. Körner, and C.-T. Tran, Analyzing new physics in the decays $\bar{B}^0 \to D^{(*)}\tau^-\bar{\nu}_\tau$ with form factors obtained from the covariant quark model, Phys. Rev. D **94**, 094028 (2016).